VOLUME 32 SEPTEMBER 1954 NUMBER 9

Canadian Journal of Physics

Editor: G. M. VOLKOFF

Associate Editors:

L. G. ELLIOTT, *Atomic Energy of Canada, Ltd., Chalk River*
J. S. FOSTER, *McGill University*
G. HERZBERG, *National Research Council of Canada*
L. LEPRINCE-RINGUET, *Ecole Polytechnique, Paris*
D. W. R. McKINLEY, *National Research Council of Canada*
B. W. SARGENT, *Queen's University*
Sir FRANCIS E. SIMON, *Clarendon Laboratory, University of Oxford*
W. H. WATSON, *University of Toronto*

Published by THE NATIONAL RESEARCH COUNCIL
OTTAWA CANADA

CANADIAN JOURNAL OF PHYSICS

(Formerly Section A, Canadian Journal of Research)

Under the authority of the Chairman of the Committee of the Privy Council on Scientific and Industrial Research, the National Research Council issues annually THE CANADIAN JOURNAL OF PHYSICS and six other journals devoted to the publication of the results of original scientific research. Matters of general policy concerning these journals are the responsibility of a joint Editorial Board consisting of: members representing the National Research Council of Canada; the Editors of the Journals; and members representing the Royal Society of Canada and four other scientific societies.

EDITORIAL BOARD

Representatives of the National Research Council

A. N. Campbell, *University of Manitoba*
G. E. Hall, *University of Western Ontario*
E. G. D. Murray, *McGill University*
D. L. Thomson, *McGill University*
W. H. Watson (Chairman), *University of Toronto*

Editors of the Journals

D. L. Bailey, *University of Toronto*
J. B. Collip, *University of Western Ontario*
E. H. Craigie, *University of Toronto*
G. A. Ledingham, *National Research Council*
Léo Marion, *National Research Council*
R. G. E. Murray, *University of Western Ontario*
G. M. Volkoff, *University of British Columbia*

Representatives of Societies

D. L. Bailey, *University of Toronto*
Royal Society of Canada
J. B. Collip, *University of Western Ontario*
Canadian Physiological Society
E. H. Craigie, *University of Toronto*
Royal Society of Canada
R. G. E. Murray, *University of Western Ontario*
Canadian Society of Microbiologists
H. G. Thode, *McMaster University*
Chemical Institute of Canada
T. Thorvaldson, *University of Saskatchewan*
Royal Society of Canada
G. M. Volkoff, *University of British Columbia*
Royal Society of Canada; Canadian Association of Physicists

Ex officio

Léo Marion (Editor-in-Chief), *National Research Council*

Manuscripts for publication should be submitted to Dr. Léo Marion, Editor-in-Chief, Canadian Journal of Physics, National Research Council, Ottawa 2, Canada.
(For instructions on preparation of copy, see **Notes to Contributors** (inside back cover).)

Proof, correspondence concerning proof, and *orders for reprints* should be sent to the Manager, Editorial Office (Research Journals), Division of Administration, National Research Council, Ottawa 2, Canada.

Subscriptions, renewals, and orders for single or back numbers should be sent to Division of Administration, National Research Council, Ottawa 2, Canada. Remittances should be made payable to the Receiver General of Canada, credit National Research Council.

The journals published, frequency of publication, and prices are:

Canadian Journal of Biochemistry and Physiology	Bimonthly	$3.00 a year
Canadian Journal of Botany	Bimonthly	$4.00 a year
Canadian Journal of Chemistry	Monthly	$5.00 a year
Canadian Journal of Microbiology*	Bimonthly	$3.00 a year
Canadian Journal of Physics	Monthly	$4.00 a year
Canadian Journal of Technology	Bimonthly	$3.00 a year
Canadian Journal of Zoology	Bimonthly	$3.00 a year

The price of single numbers of all journals is 75 cents.

*Volume 1 will combine three numbers published in 1954 with six published in 1955 and will be available at the regular annual subscription rate of $3.00.

Canadian Journal of Physics

Issued by THE NATIONAL RESEARCH COUNCIL OF CANADA

VOLUME 32 SEPTEMBER 1954 NUMBER 9

GAMMA RADIATION FROM THE PROTON BOMBARDMENT OF OXYGEN[1]

BY J. B. WARREN, K. A. LAURIE, D. B. JAMES, AND K. L. ERDMAN

ABSTRACT

The nuclear gamma radiation following the non-resonant capture of a proton in O^{16} has been studied with protons of energies from 800 kev. to 2.1 Mev. and found to consist of three components. The main transition goes, via a gamma ray of energy that varies with proton bombarding energy, to the $J = \frac{1}{2}+$ state of F^{17}. This state, 487 kev. above the ground state, radiates directly to the ground state. In addition there is a weaker direct radiative transition from the capture configuration to the ground state. At energies above $E_p = 1.8$ Mev. oxide targets bombarded with protons give rise to a radiation of 873 kev. attributed to the presence of the O^{17} isotope via the reaction $O^{17}(p, p')O^{17*}$, the radiation corresponding to the transition from the first excited state of O^{17} to the ground state.

I. INTRODUCTION

Hitherto there has been no report of the detection of nuclear gamma radiation accompanying the capture of protons by oxygen, although the production of the positron active isotope F^{17} by the reaction $O^{16}(p, \gamma)F^{17}$ has been

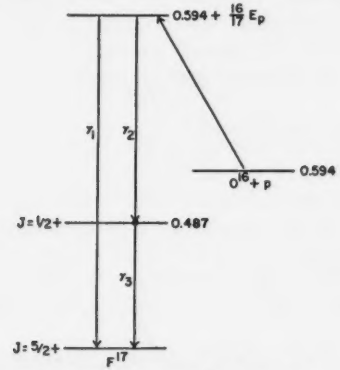

FIG. 1. Energy level diagram of F^{17}.

observed by several investigators (5, 6, 10). Energy levels in F^{17} have been determined by Laubenstein *et al.* (10) who measured the yield of the elastically scattered protons from oxygen and the capture cross-section by measuring the

[1]*Manuscript received April 7, 1954.*
Contribution from the Department of Physics, University of British Columbia, Vancouver, B.C.

activity of the F^{17} produced by proton bombardment. An assignment of angular momentum to the levels so revealed has been made by Laubenstein and Laubenstein (9). In addition information has been obtained from a study of the neutron spectrum produced in the reaction $O^{16}(d, n)F^{17}$ (1, 7), which established the existence of an excited state in F^{17} at about 0.5 Mev. above the ground state. The energy level diagram for F^{17}, and for its mirror nucleus O^{17}, with presently accepted angular momenta is given in the well-known *Energy Levels of Light Nuclei, IV* (2) and a part of this is reproduced in Fig. 1.

In this work oxygen has been bombarded with protons of energies ranging from 0.8 to 2.1 Mev., obtained from the U.B.C. electrostatic generator, and the non-resonant capture gamma radiation has been detected and measured. This has been found to correspond to the transitions marked γ_1 and γ_2 in Fig. 1, as well as to the transition, γ_3, from the first excited state to the ground state.

II. EXPERIMENTAL

(*a*) *Targets and Background*

Oxygen targets of two sorts have been used, ice deposited on a gold backing and tungsten oxide formed by heating a thin tungsten sheet in an atmosphere of pure oxygen. Both the pure gold and pure tungsten were cleaned by electrolytic etching followed by careful washing, and the "background" radiation from both of these backings was found to be adequately small in the region of gamma ray energies of main interest. A typical background spectrum is included in Fig. 2. It was found that the spectrum and intensity from the tungsten and from the gold were nearly identical in the gamma ray energy range 500 kev. to 2 Mev., and were little different from those of the cosmic ray time-dependent background. The gold gave some extra radiation in the 5 to 6 Mev. region, about four times the tungsten background, while Coulomb excitation of the low lying 'rotational' states gave rise to considerably more background intensity at and below 250 kev. for tungsten than for gold.

(*b*) *Detection*

The gamma radiation was detected by means of a scintillation counter. Two were used, one consisting of a 1 in. diam. $\times$ 1 in. high cylindrical block of sodium iodide mounted on a Dumont 6292 multiplier and the other a $1\frac{3}{4}$ in. diam. $\times$ 2 in. high block mounted on an E.M.I. 6262 multiplier. The counter was carefully and heavily shielded to reduce radiation from the electrostatic generator. Resolved proton beam currents of 6 to 8 μa. were used, the beam being defined by a gold stop to keep radiation to a minimum in the target region.

The pulse output from the counter after suitable amplification passed through a cut amplifier and was displayed on a 30 channel 'kicksorter'. The kicksorter was set up with a precision, variable pulse generator and the energy scale for the counter was established at frequent intervals using several standard sources for calibration. A careful check on the linearity of the system showed it to be better than 1% over the energy range 0.51 to 2.62 Mev.

III. RESULTS

(*a*) *The Decay of* F^{17}

A thick ice target was bombarded for several minutes and an analysis made of the gamma radiation emanating from the activity produced in the ice. No evidence for any gamma radiation, other than the annihilation radiation, was found. The background above 0.51 Mev. in this case was very low and any nuclear gamma ray of energy above 0.51 Mev. present to the extent of 3% of the annihilation radiation would, it is believed, easily have been detected.

A rather rough measurement was made of the half life of the activity produced by following the decay over several half lives using a linear rate meter (4), the output of which was fed to a Brown recorder. A value of 62.5 ± 1.0 sec. was obtained in accord with recent values (2) for the half life of F^{17}. No significant amount of any longer lived activity was detected.

(*b*) *The Capture Gamma Radiations of Variable Energy*

The gamma ray spectrum observed with protons of energy from 0.8 to 1.7 Mev. consisted of three components represented by γ_1, γ_2, γ_3 in the energy level diagram of Fig. 1. A typical spectrum, covering the gamma ray energy range from 0.6 to 2.4 Mev., obtained with a fairly thin target of tungsten oxide at $E_p = 1.355$ Mev., is shown in Fig. 2.

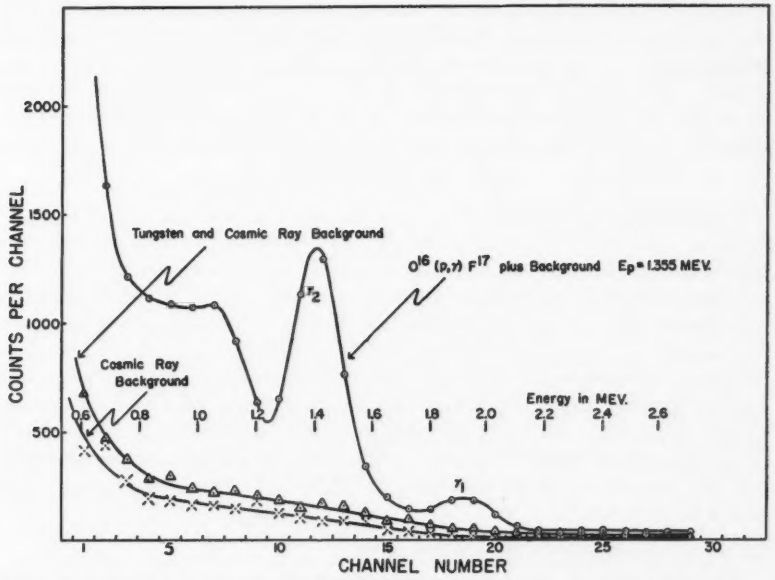

FIG. 2. Scintillation counter pulse height distribution due to radiation from a tungsten oxide target bombarded with 1.355 Mev. energy protons, together with background due to tungsten backing and time-dependent cosmic ray background.

The background radiation from a clean tungsten target and the time-dependent cosmic ray background taken under similar conditions are also shown. It is clear that two gamma rays are present, the weaker one, γ_1, corresponding to the direct transition to the ground state and the stronger one, γ_2, corresponding to a transition to a level about 487 kev. above the ground state, presumably identical to the $J = \frac{1}{2}$ even state reported by Ajzenberg (1). The energy of both these gamma rays varies with the proton bombarding energy in the manner to be expected from the energetics of the reaction. The numerical value of the gamma ray energy for the ground state transition was found to be in accord with

$$h\nu = 0.594 + (16/17)E_p \text{ in Mev.},$$

to within the experimental error of ± 15 kev., including the uncertainty as to the exact target thickness. E_p was established using the well-known 873 kev. and other resonances in the $F^{19}(p, \alpha\gamma)O^{16}$ reaction, and using the generating voltmeter to interpolate in this energy region.

The yield of both γ_1 and γ_2 increased very slowly over the energy range studied, in accord with previous measurements of the yield of F^{17} (10), and no resonance characteristics whatever were noticed. The ratio of the yield of γ_2 to γ_1 measured at 90° to the incident proton direction remained at about 10/1 over the energy range studied. Angular distribution measurements were made with difficulty on γ_1 owing to the low intensity, and all that can be stated is that no major departure from an isotropic distribution occurred at any of the energies studied. On the other hand the distribution of the γ_2 radiation was almost of the pure $\sin^2\theta$ pattern for E_p from 1.0 to 1.9 Mev. For example at $E_p = 1.90$ Mev. data taken only from 0° to 90° and uncorrected for the solid angle subtended by the crystal (0.026 of a sphere) fitted a curve of the form:

$$I(\theta) \propto 1 + (5 \pm 1)\sin^2\theta.$$

The absolute cross-section was deduced from the counter efficiency established at 1.3 Mev. using a standardized Co^{60} source and extrapolated using a Na^{22} source and a Na^{24} source, thus obtaining three points on an efficiency/quantum energy curve between which the variation could be interpolated by calculation. The ice target thickness laid down by the water vapor dispenser was established by measuring the shift in the resonance at $E_p = 1381$ kev. occurring in the $F^{19}(p, \alpha\gamma)O^{16}$ reaction when ice was laid down on a thin calcium fluoride target. By taking the stopping power of ice at this proton energy to be 6.2×10^{-15} e.v. cm.^{2} per molecule, the number of oxygen atoms present in a given target thickness could be deduced. The absolute cross-section for the production of γ_2 radiation at $E_p = 1.35$ Mev. was found to be $6 \pm 3 \times 10^{-30}$ cm.^{2}

(c) The Transition from the 487 kev. Level

The presence of a third component of energy around 0.5 Mev. was made evident, in spite of the presence of positron annihilation radiation, by examining the spectrum in the 0.5 Mev. region over various times of irradiation of the target as shown in Fig. 3. Thus the annihilation radiation activity, by the end of the first 30 sec. of a run made with a constant beam current, will only have

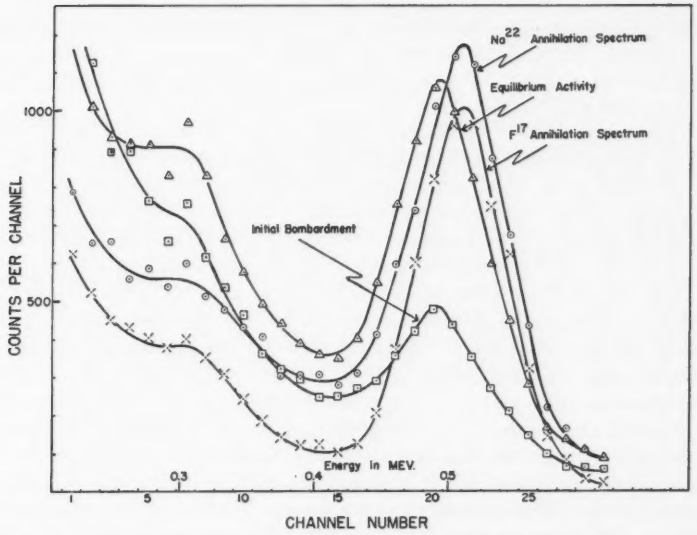

FIG. 3. Scintillation counter spectrum in 0.5 Mev. region from $O^{16}(p, \gamma)F^{17}$ reaction taken (i) during initial 30 sec. of bombardment; (ii) after equilibrium activity had been established, beam current remaining constant; (iii) after beam was cut off, due to F^{17} activity; together with (iv) a calibration, annihilation radiation peak from Na^{22}.

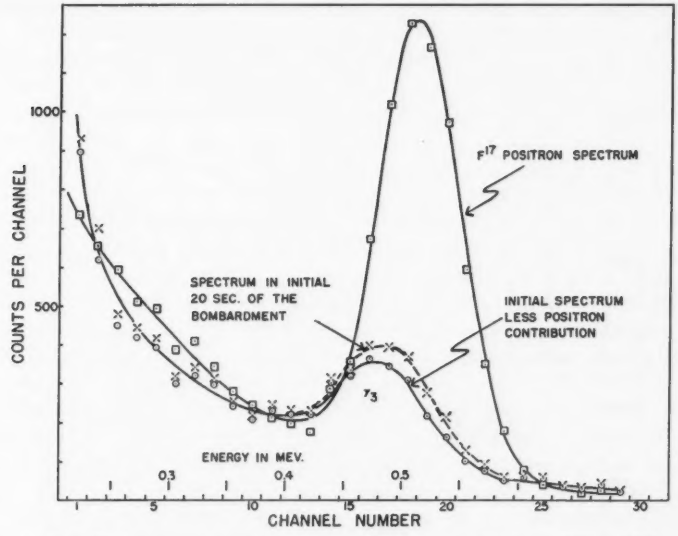

FIG. 4. Scintillation counter spectrum in the 0.5 Mev. region from $O^{16}(p, \gamma)F^{17}$ reaction taken during initial 20 sec. of a bombardment, together with the spectrum resulting after the subtraction of the annihilation radiation contribution due to the positron activity of the F^{17}. This latter contribution was 5% of the F^{17} spectrum shown, which was obtained in the 62 sec. following a 9 min. bombardment.

reached 30% of its final equilibrium activity achieved after some 10 min. bombardment. Runs made during such initial short times indicated clearly the presence of a prompt nuclear gamma ray, of energy just slightly below 0.51 Mev., the annihilation peak.

Measurements of the F^{17} positron activity, made over a half life immediately following an irradiation at constant beam current lasting some nine or ten minutes, enabled the equilibrium positron activity to be deduced, and hence the fraction of the counts due to positrons in the peak obtained during the initial period of a run to be ascertained. Thus in Fig. 4 is shown the pulse height spectrum in the 0.5 Mev. region obtained during the initial 20 sec. of a bombardment, together with the spectrum resulting after the subtraction of the positron contribution. Likewise calculation of the equilibrium annihilation radiation activity from the F^{17} activity following an irradiation showed that there were about 2.0 annihilation quanta for each 487 kev. quantum, compared to the expected value of 2.2 on the basis of a branching ratio γ_2/γ_1 of about 10/1. This small discrepancy can be accounted for by the slightly higher counter efficiency for 487 kev. than for 510 kev. radiation.

Measurements made with a thin target showed that the energy of γ_3 did not change with E_p. There was no evidence for any specially large width to this transition. The energy was below 0.51 Mev., the average value determined being 487 $\pm$ 10 kev. This is to be compared with the figure of 536 $\pm$ 10 kev. given by Ajzenberg from an analysis of the neutron groups from $O^{16}(d, n)F^{17}$ (1). It would seem very likely that the level measured is the same in both cases, since the mirror nucleus O^{17} has only one corresponding low lying state.

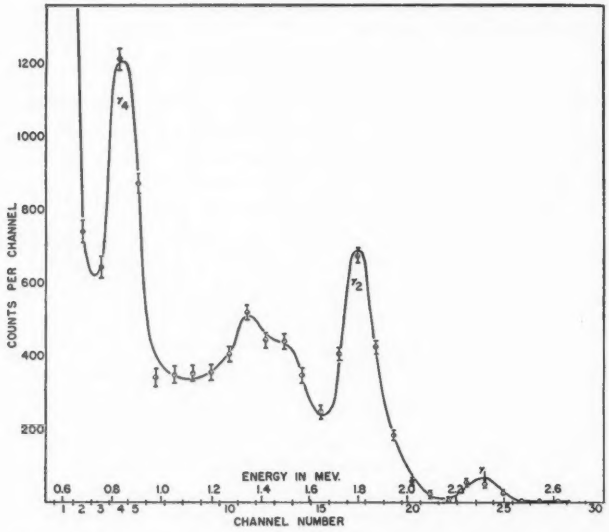

FIG. 5. Scintillation counter spectrum due to radiation from oxygen bombarded with protons of 1.898 Mev. energy, background subtracted, showing presence of 873 kev. component, γ_4.

The angular distribution of this prompt 487 kev. radiation was found to be isotropic.

(*d*) *The 873 kev. Radiation Which Appears for $E_p > 1.8$ Mev.*

Spectra taken at proton energies around 2 Mev. showed the presence of a fourth gamma ray, γ_4, Fig. 5. This gamma ray appeared with both tungsten oxide and ice targets and could not be traced to any impurity in the target or to contamination of the target from the vacuum system.

Measurements showed that the energy of this radiation did not change with E_p and that it was not detectable until E_p was raised above 1.8 Mev. Its intensity rose sharply as the proton energy was increased up to the maximum 2.1 Mev. used in this investigation. This radiation ceased as soon as the beam was turned off. The average value determined for the energy of this gamma ray is 873 ± 10 kev. Its angular distribution was found to be isotropic at $E_p = 1.9$ Mev.

IV. DISCUSSION

The absence of any prominent nuclear gamma radiation from the decay of F^{17} to O^{17} is in accord with the beta ray data of Wong (15) and indicates that only very few or none of the transitions go via the 875 kev. level of O^{17} as would be expected from the 'favored' 'allowed' character of the transition between the $5/2+$ ground states of F^{17} and O^{17}.

The gamma rays emitted during the capture of a proton by O^{16} fit the level scheme and energetically agree, within the limits of error, with the binding energy of the proton to O^{16}, deduced from the threshold of $E_d = 1.836 \pm 0.003$ Mev. for the $O^{16}(d, n)F^{17}$ reaction measured by Bonner and Butler (3). The experimental uncertainty in the measured gamma ray energies is considered to be about ± 10 kev. but in addition there is some uncertainty in the exact value of E_p due to uncertainty in target thickness; the over-all error should not exceed ± 15 kev.

The isotropic distribution of the 490 kev. gamma radiation is in accord with the previous assignment of $J = \frac{1}{2}+$ for the first excited state of F^{17} (1, 2).

However the fact that most of the transitions are found to be in cascade through the $J = \frac{1}{2}+$ state at 487 kev. shows clearly that the non-resonant gamma ray yield and capture cross-section for the production of F^{17} cannot be attributed to a broad $J = \frac{1}{2}+$ state at this low energy, as suggested by Laubenstein and Laubenstein (9). Two other explanations are possible. Firstly, if the ordinary compound nucleus theory, so successful for dealing with resonant reactions, is to be applied, then the broad states in F^{17} at 4.35 and 4.73 Mev. (10) above the ground level may be invoked to account for this yield. For example the $3/2-$ state at 4.73 Mev. would give an angular distribution of the form $(a + b \sin^2 \theta)$ in a transition to the $J = \frac{1}{2}+$ state. Since the non-resonant yield is still quite measurable at $E_p = 800$ kev., this is a rather far-fetched explanation and would still not account for the large cross-section for elastic scattering of protons at low energies (9). A second alternative and more satisfying explanation is to attribute the process to direct radiative capture, without the formation of a proper compound nucleus. There are several cases of such direct radiative capture in reactions among the lightest nuclei, for example

the $n + p \rightarrow D + \gamma$ process, the $D(p, \gamma)He^3$ and $T(p, \gamma)He^4$ reactions (8, 11, 12, 13, 14), and the $C^{12}(p, \gamma p')$ reaction (16), and it may well be that some other cases of non-resonant gamma radiation arising from simple capture in which the cross-section changes smoothly and slowly with energy are of this type.

It is even conceivable that the $\sin^2\theta$ pattern for the distribution of γ_2 may arise from the absence of spin–orbit coupling, as in the case of the $D(p, \gamma)He^3$ reaction in which the proton spin plays no significant role.

There remains the question of the origin of the radiation of 873 ± 10 kev. designated γ_4. There is little doubt that it arises from oxygen, and the measured energy value is very closely equal to that of the transition between the first excited state of O^{17} and the ground state. The isotropic angular distribution is in accord with this assignment since the first excited state of O^{17} is a $\frac{1}{2}$ even state. It seems plausible to attribute the radiation to the reaction $O^{17}(p, p')O^{17*}$, in spite of the low isotopic percentage of O^{17} present in natural oxygen, 0.04%, since such a process might well have a moderately large cross-section. (The reaction $N^{14}(\alpha, p)O^{17}$ is a prolific reaction, so that its inverse will be large, from which it is not unreasonable to expect the $O^{17}(p, p')O^{17*}$ to be observable.) The rapidly increasing yield may be attributed to the level at 7.6 Mev. in F^{18}.

It might be mentioned that the variable energy gamma rays γ_2, together with the $\frac{1}{2}$ Mev. radiation, would seem to provide a rather convenient way of establishing the relative counting efficiency of a scintillation counter for gamma radiation.

ACKNOWLEDGMENTS

We wish to thank Mr. R. E. Azuma for his help with the preliminary runs and Mr. J. Elliott for his enthusiastic assistance during the course of this experiment. We are also indebted to Professor W. Opechowski for his interest and for many helpful discussions. This work has been made possible by financial assistance from Atomic Energy of Canada Ltd.

REFERENCES

1. AJZENBERG, F. Phys. Rev. 83: 693. 1951.
2. AJZENBERG, F and LAURITSEN, T. Revs. Mod. Phys. 24: 321. 1952.
3. BONNER, T. W. and BUTLER, J. W. Phys. Rev. 83: 1091. 1951.
4. COOKE-YARBOROUGH, E. H. and PULSFORD, E. W. Proc. Inst. Elec. Engrs. (London), 98: 191. 1951.
5. CURRAN, S. C. and STROTHERS, J. E. Nature, 145: 224. 1940.
6. DU BRIDGE, L. A., BARNES, S. W., BUCK, J. H., and STRAIN, C. V. Phys. Rev. 53: 447. 1938.
7. EL BEDEWI, F. A., MIDDLETON, R., and TAI, G. T. Proc. Phys. Soc. (London), A, 64: 757. 1951.
8. GRIFFITHS, G. M. and WARREN, J. B. Phys. Rev. 92: 1084. 1953.
9. LAUBENSTEIN, R. A. and LAUBENSTEIN, M. J. W. Phys. Rev. 84: 18. 1951.
10. LAUBENSTEIN, R. A., LAUBENSTEIN, M. J. W., KOESTER, L. J., and MOBLEY, R. C. Phys. Rev. 84: 12. 1951.
11. PERRY, J. and BLAME, S. Bull. Am. Phys. Soc. 28: 51. 1953.
12. VERDE, M. Helv. Phys. Acta, 23: 453. 1950.
13. WARREN, J. B. and GRIFFITHS, G. M. Phys. Rev. 92: 1084. 1953.
14. WILKINSON, D. H. Phil. Mag. 43: 659. 1952.
15. WONG, C. Bull. Am. Phys. Soc. 27: F. 9. Dec. 26, 1952, meeting.
16. WOODBURY, H. H., TOLLESTRUP, A. V., and DAY, R. B. Phys. Rev. 93: 1311. 1954.

REFLECTION FROM A WIRE GRID PARALLEL TO A CONDUCTING PLANE[1]

By James R. Wait

ABSTRACT

A solution is outlined for the problem of a plane wave incident obliquely on a parallel-wire grid which is backed by a plane conducting surface. The electric vector of the incident wave is taken to be parallel to the grid wires. The equivalent transmission line problem is pointed out. It is shown that, in certain cases, a resistive wire grid will absorb all the energy in the incident wave.

INTRODUCTION

There have been numerous investigations of the electromagnetic properties of a grating of thin parallel cylindrical wires composed of conductive material. Such gratings have been employed to shield regions from spurious electromagnetic fields or to act as reflectors in antenna systems to simulate a reflecting plane surface. The first quantitative study was made by Lamb (6) in 1898 who considered a plane wave incident normally on a grid. He showed that if the spacing between the parallel wires was small, the reflection and transmission of the waves could be varied by changing the wire radius.

In 1914 von Ignatowsky (5) made a very exhaustive analysis of the scattering of incident plane waves by single, infinite metallic grids. His formulas have been rededuced, extended, and applied by other authors (3, 4, 7, 9, 12, 13) since that time. A very illuminating treatment has been given by MacFarlane (8) who indicated that a single grid can be represented by an impedance shunted across an infinite transmission line whose characteristic impedance is equal to the intrinsic impedance of free space. He showed that this impedance, for any grid spacing, was proportional to $(\log(d/2\pi a)+F)$ where a is the wire radius and F is a correction factor which is a function of the angle of incidence and the spacing d.

It is the purpose of this paper to consider the case of reflection of plane waves from a wire grid which is parallel to a conducting wall. In this case it can be anticipated that the grid may still be represented by a shunt impedance whose value, however, will depend to a certain extent on the distance to the conducting plane. It will be shown in this paper that the shunt impedance is proportional to $(\log(d/2\pi a)+\Delta)$ where Δ is now a function of the angle of incidence, grid spacing wavelength ratio, and the distance of the grid to the conducting plane. The resultant reflection coefficient can then be found directly by representing the conducting wall as a short circuit across the equivalent transmission line mentioned above.

The possibility of modifying the properties of the grid by inserting small resistors in the wires is also discussed. It appears that under certain conditions the reflection coefficient can be made to vanish if the distance to the conducting plane behind the grid is properly chosen.

[1]*Manuscript received May 14, 1954.*
Contribution from the Radio Physics Laboratory, Defence Research Board, Ottawa, Ont.

GENERAL THEORY

With respect to a Cartesian coordinate system the wire grid is contained in the plane $x = h$ and is backed by a perfectly conducting wall at $x = 0$. The grid is composed of an array of wires parallel to the axis and spaced a distance d between centers. The wires are taken to be of circular cross section and are assumed initially to be of infinite conductivity. The insulating space ($x > 0$) surrounding the wire grid is homogeneous and has a dielectric constant ϵ_0 and permeability μ_0.

A plane wave with the electric field of magnitude E_0 parallel to the z axis impinges on the grid with angle of incidence θ as indicated in Fig. 1*a*. The primary or incident field is given by

$$E_i = E_0 \exp[i2\pi\lambda^{-1}(x \cos\theta + y \sin\theta)] \qquad [1a]$$

where the time factor $\exp(i\omega t)$ has been omitted and

$$2\pi\lambda^{-1} = (\epsilon_0\mu_0)^{\frac{1}{2}}\omega$$

where λ is the wavelength. The currents induced on the wires will all be of equal magnitude I but will have a progressive change of phase between adjacent wires of $2\pi\lambda^{-1}d \sin\theta$ radians. The phase of the wire at $x = h$, $y = 0$

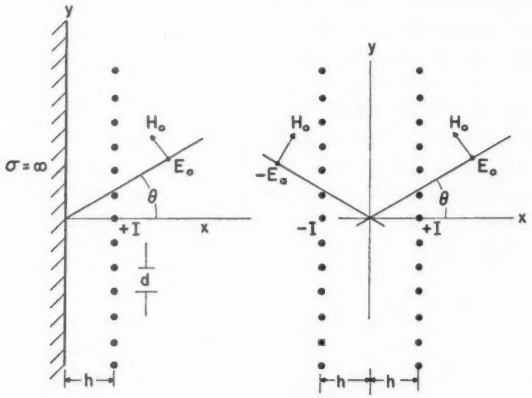

FIG. 1(*a*). The parallel wire grid and the conducting plane.
(*b*). The equivalent problem employing the image principle.

can be arbitrarily zero. The incident wave will also be reflected from the conducting plane at $x = 0$. To calculate the magnitude of the current I on the wire and the resultant reflected fields it is convenient to apply the theorem of images.

The conducting plane and the wire grid are replaced by two identical wire grids contained in the planes $x = \pm h$ as shown in Fig. 1*b*. To satisfy the boundary condition that the electric field should vanish on the plane $x = 0$ a reflected wave has the form

[1b] $$E_r = -E_0 \exp[i2\pi\lambda^{-1}(-x\cos\theta + y\sin\theta)]$$

and in addition the currents on the image grid at $x = -h$ must be equal and opposite to the currents on the grid at $x = h$.

The problem is now to find the field at a point $P(x, y)$ as a result of scattering of the two plane waves from the double grid system. It is assumed that the wires are of small diameter compared with the spacing and with the distance to the conducting plane, that is $d \gg a$ and $h \gg a$. The parallel field E at a distance R from an infinite wire carrying a current I is well known (3) and is given by

[2] $$E = \tfrac{1}{4}\mu_0\omega I H_0^{(2)}(2\pi\lambda^{-1}R)$$

where $H_0^{(2)}$ is the Hankel function of the second type and is chosen to give rise to outgoing waves at infinity for a time factor $\exp(i\omega t)$. The field E_w at P due to the currents flowing in the wire grid at $x = h$ is then

[3] $$E_w = \frac{\mu_0\omega I}{4}\sum_{n=-\infty}^{+\infty} e^{i2\pi n\lambda^{-1}d\sin\theta} H_0^{(2)}[2\pi\lambda^{-1}\sqrt{\{(nd-y)^2 + (x-h)^2\}}]$$

which can be transformed to a more convergent summation (see Appendix), as follows:

[4] $$E_w = \frac{i\mu_0\omega I}{4\pi} e^{i2\pi\lambda^{-1}y\sin\theta}\sum_{m=-\infty}^{+\infty} e^{i2\pi m y d^{-1}} \frac{e^{-2\pi(x-h)d^{-1}\sqrt{[(m+D\sin\theta)^2 - D^2]}}}{\sqrt{[(m + D\sin\theta)^2 - D^2]}}$$

where $D = d/\lambda$. Correspondingly, the field E_w' at P due to the currents flowing in the wire grid at $x = -h$ is given by

[5] $$E_w' = -\frac{i\mu_0\omega I}{4\pi} e^{i2\pi\lambda^{-1}y\sin\theta}\sum_{m=-\infty}^{+\infty} e^{i2\pi m y d^{-1}} \frac{e^{-2\pi(x+h)d^{-1}\sqrt{[(m+D\sin\theta)^2 - D^2]}}}{\sqrt{[(m + D\sin\theta)^2 - D^2]}}.$$

The total field E at P is then

[6] $$E = E_i + E_r + E_w + E_w'.$$

It can be seen by inspection that $E = 0$ at the plane $x = 0$. The value of the current I is now found from the boundary condition that the field E must also be zero on the surface of the wires of the grid. The point P is taken therefore to be at $x = h + a$ and $y = 0$, and the equation for I becomes

[7] $$E_0(e^{i2\pi\lambda^{-1}h\cos\theta} - e^{-i2\pi\lambda^{-1}h\cos\theta}) + (I/d)[(\eta_0/2\cos\theta)(1 - e^{-i4\pi\lambda^{-1}h\cos\theta}) + Z_g] = 0$$

where

[8] $$Z_g = \frac{i\mu_0\omega d}{2\pi}\left[\log\frac{d}{2\pi a} + \Delta\right] \text{ and } \eta_0 = (\mu_0/\epsilon_0)^{\frac{1}{2}} \simeq 120\pi$$

with

[9] $$\Delta = \frac{1}{2}\sum_{m=1}^{\infty}\left[\frac{1 - e^{-4\pi HD^{-1}\sqrt{[(m+D\sin\theta)^2 - D^2]}}}{\sqrt{[(m + D\sin\theta)^2 - D^2]}} + \frac{1 - e^{-4\pi HD^{-1}\sqrt{[(m-D\sin\theta)^2 - D^2]}}}{\sqrt{[(m - D\sin\theta)^2 - D^2]}} - \frac{2}{m}\right]$$

where $D = d/\lambda$, $H = h/\lambda$, and it has been assumed that $d \gg a$. The current I on the reference wire at $x = h$, $y = 0$ is then expressed in terms of the incident field E_0 by

$$I = \frac{-2id[\sin(2\pi H\cos\theta)]\,E_0}{(\eta_0/2\cos\theta)(1 - e^{-i4\pi H\cos\theta}) + Z_g}. \tag{10}$$

This result along with equations [3] to [6] constitutes the solution of the problem. The restriction to infinite conductivity of the wires composing the grid can be removed if the boundary condition $E = 0$ on the wires is replaced by the condition

$$E = -Iz_i \tag{11}$$

where z_i is the internal impedance of the wire. It can be assumed that the field is uniform around the wire since $a \ll d$ and $a \ll h$, and hence z_i can be calculated by known methods (10) and is given by

$$z_i = \frac{\eta\, I_0(\gamma a)}{2\pi a\, I_1(\gamma a)} \tag{12}$$

where $\eta = [i\mu\omega/(\sigma + i\omega\epsilon)]^{\frac{1}{2}}$ and $\gamma = [i\mu\omega(\sigma + i\omega\epsilon)]^{\frac{1}{2}}$ and μ, σ, and ϵ are the permeability, conductivity, and dielectric constant of the wire material. I_0 and I_1 are modified Bessel functions of order zero and unity. For metallic wires the displacement currents are negligible since $\omega\epsilon \ll \sigma$ even at microwave frequencies. In addition, the frequency is usually sufficiently high so that $|\gamma a| \gg 1$ and hence

$$z_i \simeq \left(\frac{\mu\omega}{2\sigma}\right)^{\frac{1}{2}} \frac{1+i}{2\pi a}.$$

Employing this result it follows that the defining equation for Z_g should read

$$Z_g = \frac{i\mu_0\omega d}{2\pi}\left(\log\frac{d}{2\pi a} + \Delta\right) + (1+i)\frac{d}{2\pi a}\left(\frac{\mu\omega}{2\sigma}\right)^{\frac{1}{2}} \tag{13}$$

which reduces to equation [8] for the case of $\sigma = \infty$.

THE DISTANT FIELD

The case of particular interest is that in which the field point is sufficiently far removed from the grid so that $(x - h) \gg \lambda$. On inspection of equations [3] and [4] for the field E_w and E_w' it is evident that only the term $m = 0$ is significant for $d/\lambda < 1/(1 + \sin|\theta|)$. The higher values of m correspond to evanescent waves which are highly damped in the positive x direction. For larger values of d/λ, additional undamped waves can be scattered from the grid. The discussion will be limited here, however, to the smaller grid spacings satisfying the above inequality. The field at P can then be written as follows:

$$E = E_0\, e^{i2\pi\lambda^{-1}(x\cos\theta + y\sin\theta)} + \left[-E_0 + \frac{I\eta_0}{2d\cos\theta}(e^{i2\pi H\cos\theta} - e^{-i2\pi H\cos\theta})\right] e^{i2\pi\lambda^{-1}(-x\cos\theta + y\sin\theta)}. \tag{14}$$

Employing equation [10] this is written

$$E = E_0\, e^{i2\pi\lambda^{-1}y\sin\theta}(e^{i2\pi\lambda^{-1}x\cos\theta} + Re^{-i2\pi\lambda^{-1}x\cos\theta}) \quad [15]$$

where

$$R = -1 + \frac{(2\eta_0/\cos\theta)\sin^2(2\pi H\cos\theta)}{(\eta_0/2\cos\theta)(1 - e^{-i4\pi H\cos\theta}) + Z_g}. \quad [16]$$

Evidently the first term in [16] is the reflection coefficient of a plane conducting surface whereas the second term represents the effect imposed by the presence of the wire grid.

Fig. 2 illustrates an electrical circuit which may be taken as the analogue of the wire grid and conducting surface.

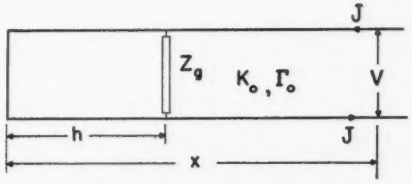

FIG. 2. The analogous electrical transmission line.

The space to the right of the plane $x = 0$ is represented by a transmission line whose characteristic impedance is K_0 and whose propagation constant is Γ_0. The conducting plane is represented by a short circuit at $x = 0$. At a distance h from the shorted end is an impedance Z_g shunted across the line. The voltage V is considered to be due to the superposition of the two travelling waves, so that

$$V = V_0(e^{\Gamma_0 x} + Re^{-\Gamma_0 x}) \quad [17]$$

and the current J at x is therefore

$$J = (V_0/K_0)(e^{\Gamma_0 x} - Re^{-\Gamma_0 x}). \quad [18]$$

It can be verified readily from transmission line theory that R is given by equation [16] if

$$K_0 = \eta_0/\cos\theta, \qquad V_0 = E_0, \qquad \Gamma_0 = i2\pi\lambda^{-1}\cos\theta.$$

V and J are then identified with the electric field E and the magnetic field component H_y respectively.

The factor Z_g can now be termed the shunt impedance of the grid and is given by equation [13]. It can be seen that for $d \ll \lambda$ and $d \ll h$ the factor Δ is negligible compared with $\log(d/2\pi a)$ and therefore

$$Z_g = i\eta_0 \frac{d}{\lambda}\log\frac{d}{2\pi a} + dz_t, \quad [19]$$

which is identical with the expression for the impedance of a single resistive wire grid in free space for the case $d \ll \lambda$ and normal incidence given by Gans (2).

It is apparent therefore that the grid possesses a shunt impedance which is mainly a function of d/λ and wire radius a and which depends to a lesser extent on the angle of incidence and the presence of the conducting surface. Values of the correction factor Δ are plotted in Fig. 3(a) to (d) as a function of h/λ for various values of d/λ and θ.

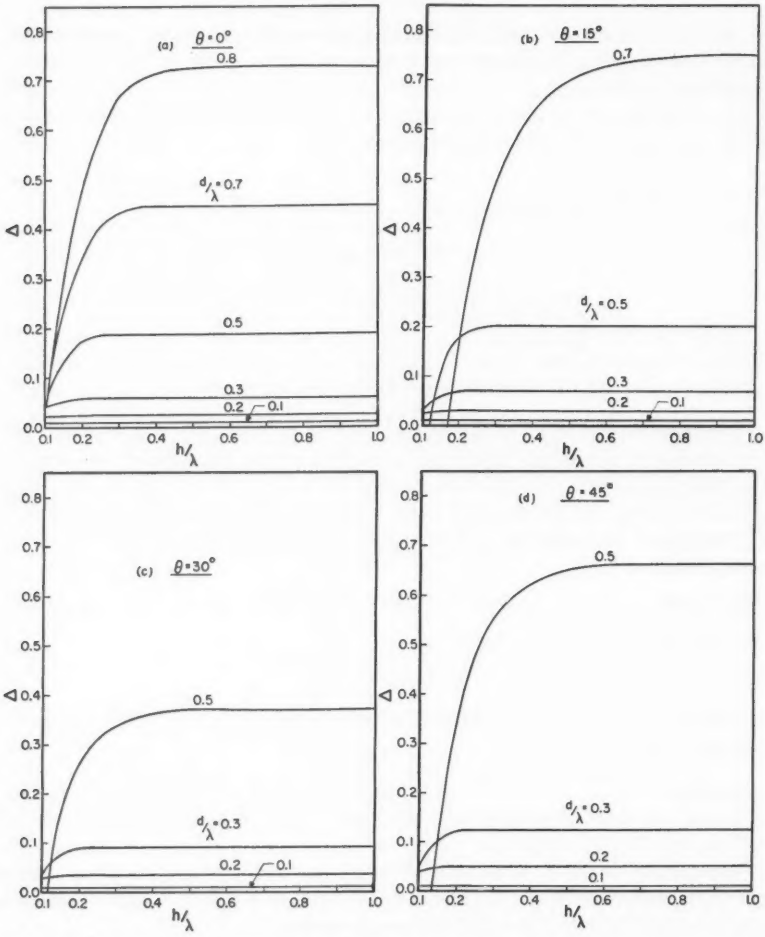

FIG. 3. The correction factor Δ as a function of the distance of the grid to the conducting plane for a specified angle of incidence.

AN APPLICATION

A possible application of this analysis is to the design of a simulated anti-reflective coating, for by letting

[20] $$Z_g = iX_g + R_g$$

where X_g and R_g are the shunt reactance and shunt resistance of the grid, it can be seen easily from equation [16] that if $R = 0$, then

[21] $$X_g = -(\eta_0/2\cos\theta)\sin(4\pi H\cos\theta)$$

and

[22] $$R_g = (\eta_0/\cos\theta)\sin^2(2\pi H\cos\theta)$$

where equation [22] immediately implies that the wires must possess a finite conductivity or otherwise be modified to absorb the energy of the incident wave.

The equation for the reactance, for the case $d/\lambda < 1/(1 + \sin|\theta|)$, is then written as follows:

[23] $$\sin(4\pi H\cos\theta) = -\frac{\eta_0(d/\lambda)(\log(d/2\pi a) + \Delta)}{(\eta_0/2\cos\theta)}.$$

It is apparent that the sine must be negative, therefore H lies in the range defined by $\frac{1}{2}N > H\cos\theta > \frac{1}{4}(2N - 1)$ for $N = 1, 2, 3 \ldots$.

For a conducting grid fabricated from metal wires the actual resistance R_g will usually be much smaller than specified by equation [22]. It should be a relatively simple matter, however, to modify R_g by inserting small carbon resistors of r ohms at regular intervals s along each of the wires. For $d \ll \lambda$ and $s \ll \lambda$ it can be seen that

[24] $$R_g = \frac{d}{s}r + \left(\frac{\mu\omega}{2\sigma}\right)^{\frac{1}{2}}\frac{d}{2\pi a}$$

where the second term, which is the effective resistance of the wire, would be small compared with the first term. The required value of r for a vanishing reflection coefficient is then given by

[25] $$r \simeq \frac{s}{d}\left(\frac{\eta_0}{\cos\theta}\right)\sin^2(2\pi H\cos\theta) - \left(\frac{\mu\omega}{2\sigma}\right)^{\frac{1}{2}}\frac{s}{2\pi a}.$$

Equations [23] and [25] can be employed to calculate the required value of h/λ and r for zero reflection having specified values of d, σ, μ, θ, and a. When the grid spacing becomes small, however, such that $d \ll \lambda$, the design equations become much simpler. In this case $h\cos\theta$ is slightly greater than an odd number of quarter wavelengths or slightly less than an integral number of half wavelengths. For example if

[26] $$h = \frac{(2N - 1)\lambda}{4\cos\theta} + \delta_1$$

or

[27] $$h = \frac{N\lambda}{2\cos\theta} - \delta_2$$

for $N = 1, 2, 3 \ldots$, then δ_1 and δ_2 are small compared with λ, since $\sin(4\pi H\cos\theta)$ is a small quantity compared with unity if $d \ll \lambda$. To this order of approximation it follows from equations [22] and [25] that

$$\delta_1 = \delta_2 = \frac{d}{2\pi}\log\frac{d}{2\pi a} + \left(\frac{\mu\omega}{2\sigma}\right)^{\frac{1}{2}}\frac{\lambda d}{4\pi^2 a} \tag{28}$$

and

$$r \simeq \frac{s}{d}\frac{\eta_0}{\cos\theta} - \left(\frac{\mu\omega}{2\sigma}\right)^{\frac{1}{2}}\frac{s}{2\pi a} \tag{29}$$

for the conditions of equation [26] and

$$r \simeq \frac{s}{d}\frac{\eta_0}{\cos\theta}(2\pi H\cos\theta)^2 - \left(\frac{\mu\omega}{2\sigma}\right)^{\frac{1}{2}}\frac{s}{2\pi a} \tag{30}$$

for the conditions of equation [27].

An experimental study of wire grids backed by conducting and dielectric media is being carried out in this laboratory. The results will be reported at a later date.

APPENDIX

A Summation Formula

A derivation is given here for the relations expressed by equations [3] and [4]. The starting point is Poisson's formula

$$\sum_{m=-\infty}^{+\infty} H(m) = \sum_{n=-\infty}^{+\infty} h(n) \tag{31}$$

where

$$H(m) = \int_{-\infty}^{+\infty} h(x)\, e^{i2\pi mx}dx. \tag{32}$$

This formula is valid if $h(x)$ is integrable in the interval $(-\infty, +\infty)$, continuous, and steadily decreasing to zero as $x \to \infty$ and $H(m)$ is the Fourier transform of $h(x)$. Letting

$$h(x) = e^{i2\pi k(x-\delta)}H_0^{(2)}(2\pi\alpha\sqrt{[(x-\delta)^2 + \epsilon^2]}) \tag{33}$$

and setting $x = y + \delta$ it follows that

$$\begin{aligned} H(m) &= e^{i2\pi m\delta}\int_{-\infty}^{+\infty} e^{i2\pi(m+k)y}H_0^{(2)}[2\pi\alpha\sqrt{(y^2+\epsilon^2)}]\,dy \\ &= ie^{i2\pi m\delta}\frac{e^{-2\pi\epsilon\sqrt{[(m+k)^2-\alpha^2]}}}{\pi\sqrt{[(m+k)^2-\alpha^2]}} \end{aligned} \tag{34}$$

where use has been made of a formula of Campbell and Foster (1) (No. 917 with $p = i2\pi y$, $g = m + k$, $\sigma = i\alpha$, and $\rho = 2\pi\epsilon$). The required formula is now given by

$$\begin{aligned} &\sum_{n=-\infty}^{+\infty} e^{i2\pi kn}H_0^{(2)}[2\pi\alpha\sqrt{\{(n-\delta)^2+\epsilon^2\}}] \\ &\qquad = \frac{i}{\pi}e^{i2\pi k\delta}\sum_{m=-\infty}^{+\infty}\frac{e^{i2\pi m\delta}e^{-2\pi\epsilon\sqrt{[(m+k)^2-\alpha^2]}}}{\sqrt{[(m+k)^2-\alpha^2]}}. \end{aligned} \tag{35}$$

When δ is set equal to zero the above equation reduces to a formula derived

by Smith, Infeld, and Chien (11). When ϵ is also allowed to approach zero it follows that

$$[36] \quad 2\pi \sum_{m=1}^{\infty} \cos(2\pi kn)\, H_0^{(2)}(2\pi\alpha n) = -\pi + 2i \log \tfrac{1}{2}K\alpha + \frac{i}{\sqrt{(k^2-\alpha^2)}} + i\sum_{m=1}^{\infty}\left[\frac{1}{\sqrt{[(m+k)^2-\alpha^2]}} + \frac{1}{\sqrt{[(m-k)^2-\alpha^2]}} - \frac{2}{m}\right]$$

where $\log K = 0.5772\ldots$, which is Euler's number. The special case of equation [36] where $k = 0$ was given originally by Ignatowsky (5).

ACKNOWLEDGMENTS

I would like to thank Dr. P. A. Forsyth who read the manuscript and made several useful suggestions. Appreciation should also be expressed to Mr. W. A. Pope who carried out the numerical computations.

REFERENCES

1. Campbell, C. A. and Foster, R. M. Fourier integrals for practical applications. D. Van Nostrand Company, Inc., New York. 1948. p. 125.
2. Gans, R. Ann. Physik, 61: 447. 1920.
3. Groves, W. E. J. Appl. Phys. 24: 845. 1953.
4. Honerjager, R. Ann. Physik, 4: 25. 1948.
5. Ignatowsky, W. von. Ann. Physik, 44: 369. 1914.
6. Lamb, H. Proc. London Math. Soc. 29: 523. 1898.
7. Lewis, E. and Casey, J. J. Appl. Phys. 23: 605. 1952.
8. MacFarlane, C. G. J. Inst. Elec. Engrs. (London), 93 (111*a*): 1523. 1946.
9. Marcuvitz, N. Waveguide handbook. McGraw-Hill Book Company, Inc., New York. 1951. p. 286.
10. Schelkunoff, S. A. Electromagnetic waves. D. Van Nostrand Company, Inc., New York. 1943. p. 264.
11. Smith, V. G., Infeld, L., and Chien, W. J. Math. and Phys. 26: 22. 1947.
12. Trentini, G. von. Z. angew. Phys. 5: 221. 1953.
13. Wessel, W. Hochfrequenztechnik, 54: 62. 1939.

THE PHOTONEUTRON AND PHOTOPROTON CROSS SECTIONS OF SILICON AND MAGNESIUM[1]

By L. Katz, R. N. H. Haslam, J. Goldemberg,[2] and J. G. V. Taylor[3]

ABSTRACT

The (γ, n) and (γ, p) cross sections were measured as a function of photon energy in a number of isotopes. They were found to have the resonance shapes characteristic of photonuclear reaction for which the pertinent data are summarized in the table.

Isotope	Reaction	Threshold (Mev.)	Position of peak (Mev.)	Maximum cross section (mbarns)	Integrated cross section (Mev-barn)
Mg^{25}	(γ, n)	7.2	~13	~14	~0.05
	(γ, p)	12.1	20.5	27	0.12
Mg^{26}	(γ, n)	11.1	~17	~30	~0.09
	(γ, p)	14.3	22	25	0.07
Si^{29}	(γ, n)	8.5 and 10.6	15	23	0.096
$+Si^{30}$	(γ, p)	12.3 and 12.9	21	32	0.23

In view of the fact that in each isotope the threshold for the (γ, p) reaction is higher than that for the (γ, n) reaction it is surprising to find the maximum (γ, p) cross section to be at least equal to the maximum (γ, n) cross section, while peaking at about 6 Mev. higher energy. These results are discussed in some detail.

1. INTRODUCTION

The applicability of Weisskopf's statistical nucleus theory (32) to photonuclear reactions in the energy region up to 30 Mev. is still much in question. Considerable evidence may be found in the literature for its apparent failure. For instance, the energy spectrum of protons emitted in photodisintegration experiments seems to indicate a high energy tail (5, 31) not expected from the statistical theory. Measurements on the angular distribution of the emitted protons and neutrons seem to indicate anisotropy in some cases (4, 31, 12), a fact which is not easily reconciled with statistical theory. Again, experiments at Zürich (11) with γ-rays from the $Li^7(p, \gamma)Be^8$ reaction of energy 14.8 and 17.6 Mev. indicate a greater ratio of proton to neutron reactions than is predicted by the statistical theory. In all these cases however the deviations from the statistical theory involved a relatively small fraction of the total number of reactions occurring. For example, the number of protons in the high energy tail (5) of the proton spectrum is a relatively small fraction of the protons involved.

To explain these discrepancies Courant (3) and Marquez (20) proposed that, in addition to the usual Goldhaber–Teller (8) type of interaction which always

[1]*Manuscript received May 31, 1954.*
Contribution from the Department of Physics, University of Saskatchewan, Saskatoon, Sask.
[2]*Now at Department of Physics, University of São Paulo, São Paulo, Brazil.*
[3]*Now at Department of Physics, Hamilton College, Hamilton, Ont.*

results in a compound nucleus, in some cases a photon is absorbed by one proton in the nucleus, which is then emitted without the formation of an intermediate compound nucleus. According to Courant the protons emitted in the direct process are usually "masked" by the statistical protons. They should be most easily observed in nuclides whose (γ, p) threshold is not much lower than the (γ, n) threshold. This precisely is the case in the elements examined by Hirzel and Wäffler (11), and a relatively small contribution from the direct process is sufficient to explain their results as Courant has shown. It must be pointed out however that the measurements of Hirzel and Wäffler refer to (γ, n) and (γ, p) processes in different isotopes of the same element. It has been found that strong fluctuations may occur in the photo cross sections in such cases and their comparison must be interpreted with some care. Similarly a small contribution from the direct process will serve to explain the high energy proton tail observed by Diven and Almy (5).

It would be desirable to compare (γ, n) and (γ, p) cross sections in the same isotope. Outside of the measurements of Halpern and Mann (9) and of Toms and Stephens (31), very few (γ, p) cross sections are available for such comparison. These workers have published the (γ, p) cross sections for C^{12}, Al^{27}, Ni^{58}, Co^{59}, Nb^{93}, In^{115}, Ce^{133}, and Bi^{209}. Gamma–neutron cross sections in some of these elements have been measured in our laboratory (21, 7) so that intercomparison is possible in these cases. It turned out that the measured ratio $\sigma_{\gamma,p}/\sigma_{\gamma,n}$ was quite satisfactory when compared with that expected from statistical theory, except possibly for the case of Nb^{93}. An analysis of the thresholds for these elements brought to light the fact that in all cases examined the (γ, p) threshold was lower than the (γ, n) threshold by at least 2 Mev. Some of these thresholds are given in Table I.

TABLE I

THRESHOLDS FOR (γ, p) AND (γ, n) REACTIONS OF THE ISOTOPES INDICATED (MEV.)

Element	(γ, p)	Ref.	(γ, n)	Ref.
C^{12}	15.95	(19)	18.7	(19)
Al^{27}	8.26	(18)	12.75	(28)
Co^{59}	7.64	(13)	10.25	(28)
Ni^{58}	7.5	(9)	11.7	(13)
Ni^{60}	8.8	(9)	11.6	(13)
Nb^{93}	6.3	(9)	8.7	(28)

This particular sequence of thresholds favors the emission of protons by the excited nuclei. Protons resulting from the direct process would not in this case be so easily detected. It is immediately seen that an examination of some isotopes in which the (γ, p) threshold is higher than the (γ, n) threshold would be of great interest. Fortunately, the low percentage isotopes in magnesium and silicon present two such cases, as can be seen from Table II. For this reason these cross sections have been measured and the results are presented in this paper.

TABLE II

PHOTONUCLEAR THRESHOLDS IN THE MAGNESIUM AND SILICON ISOTOPES (18) (MEV.)

Isotope	Abundance, %	(γ, p)	(γ, n)
Mg^{24}	78.8	11.7	16.6
Mg^{25}	10.1	12.1	7.2
Mg^{26}	11.1	14.3	11.1
Si^{28}	92.2	11.6	16.9
Si^{29}	4.7	12.3	8.5
Si^{30}	3.1	12.9	10.6

2. EXPERIMENTAL PROCEDURE AND RESULTS

(a) *Silicon*

The (γ, p) reactions in Si^{29} and Si^{30} lead to Al^{28}, 2.3 min. half-life, and Al^{29}, 6.6 min. half-life. One-gram samples of silicon powder 99.87% pure were irradiated in a cadmium thimble inside a lucite block. After irradiation the decay curves of the silicon powder were measured and resolved into 2.3 and 6.6 min. components. No other activity was observed.

Absolute determination of the activities was carried out at 22 Mev. using the $Cu^{63}(\gamma, n)Cu^{62}$ reaction as a standard. Samples thick enough to give a cosine distribution of the emitted β rays were used and the procedure outlined by Baker and Katz (1) was followed. The decay scheme used for Al^{28} was that of Motz and Alburger (22) and for Al^{29}, that of Seidlitz, Bleuler, and Tendam (26). The uncertainty in the branching ratio in the disintegration scheme of Al^{29} will result in an uncertainty of about 5% in this activation curve. The absolute values of the cross sections are thought to be accurate to within 20%,

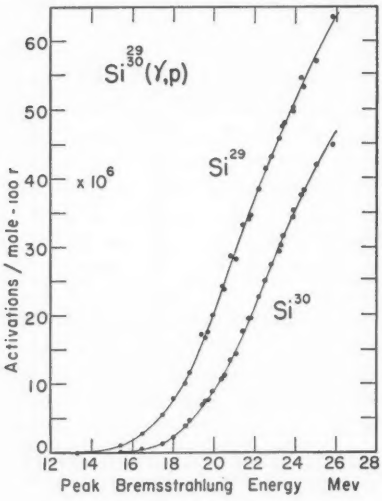

FIG. 1. Activation curves resulting from (γ, p) reactions in Si^{29} and Si^{30}.

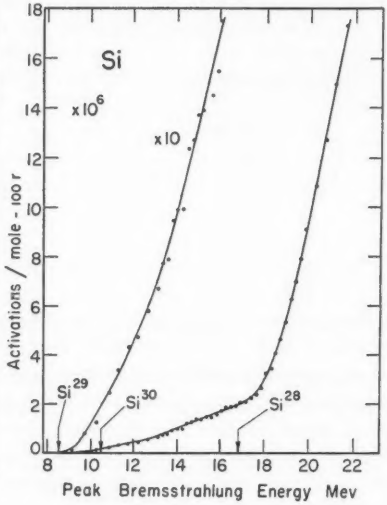

FIG. 2. Neutron yield from natural silicon.

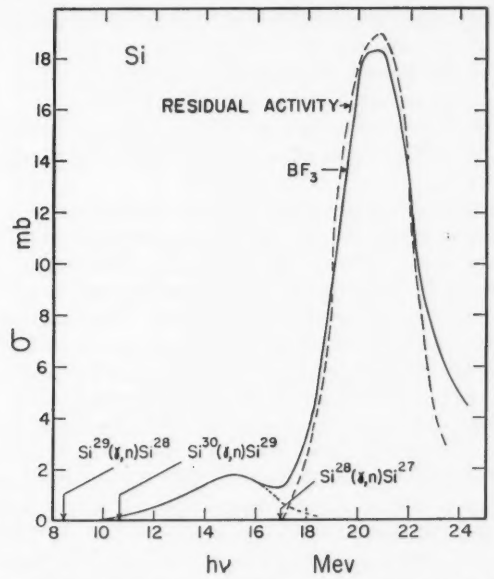

FIG. 3. Photoneutron cross section of natural silicon. The dashed curve represents the (γ, n) cross section of Si^{28}, corrected for isotopic abundance, as measured by Summers-Gill *et al.* (29).

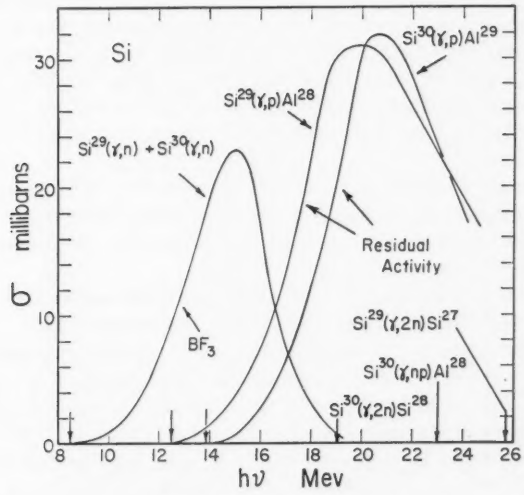

FIG. 4. Photo cross sections of Si^{29} and Si^{30}. The (γ, n) curve has been normalized per mole of these isotopes mixed according to their isotopic abundance. The (γ, p) curves are per mole of the respective isotopes.

which is the figure usually quoted in our measurements and which has been substantiated by measurements in other laboratories. The relative cross sections are probably known with somewhat greater precision. The positions of peak cross section are established to within 1 Mev.

The activation curves are shown in Fig. 1; they were solved for the cross sections using the "photon difference method" (15). The results are shown in Fig. 4.

The (γ, n) reactions cannot be measured by residual activity since the end products of the reactions are stable. For these measurements we therefore used a method which detected the emitted neutrons. This method has been previously described (21). It has the inconvenience of giving the total cross section for natural silicon. Advantage was taken, however, of the fact that the threshold for the (γ, n) reaction in the main isotope, Si^{28}, is very high (29) (16.9 Mev.). Thresholds for the other isotopes are much lower so the neutron yield curve exhibits the peculiar shape shown in Fig. 2. Normalization of this curve was carried out against copper at a number of energies. The cross section obtained is shown in Fig. 3. The cross section obtained by Summers-Gill *et al.* (29) for the reaction $Si^{28}(\gamma, n)Si^{27}$ properly corrected for isotopic abundance is shown in the same figure by a dashed curve. There is excellent agreement between both curves above the threshold for the (γ, n) reaction in Si^{28}; hence the little "bump" in the cross section of Fig. 3 is attributed to the (γ, n) reactions in Si^{29} and Si^{30}. No separation of the components is here possible.

(*b*) *Magnesium*

To measure the (γ, p) cross sections in magnesium, thin disks of this material were irradiated in the betatron beam at various energies and counted after the 12 sec. activity resulting from the (γ, n) reaction in Mg^{24} had died out. The decay curve obtained had a 62 sec. component from the $Mg^{26}(\gamma, p)Na^{25}$ reaction and a 14.9 hr. component from the $Mg^{25}(\gamma, p)Na^{24}$ reaction. The activation curves were normalized to the known $Cu^{63}(\gamma, n)Cu^{62}$ yield at 22 Mev. after making the necessary corrections for self-absorption (1) and decay scheme (23).

These normalized activation curves are shown in Fig. 5. They were analyzed by the photon difference method and yielded the cross section curves shown in Fig. 9. Comparison of these cross sections to previously published values will be made in Section 3.

As in the case of silicon, the (γ, n) cross sections were measured by detecting the neutrons resulting from these reactions. The neutron yield curve, standardized against the neutron yield from the (γ, n) reaction in copper according to our usual procedure (21), is shown in Fig. 6. Analyzing this curve by the photon difference method resulted in the cross section curve shown in Fig. 7. This cross section is of course the sum of the (γ, n) cross sections in the three isotopes; however the large peak above 16.6 Mev. must be due to the 78.8% isotope Mg^{24} which has its threshold at this energy.

The cross section for this isotope had been previously measured by Katz and Cameron (16) by detecting the 12 sec. Mg^{23} activity resulting from the

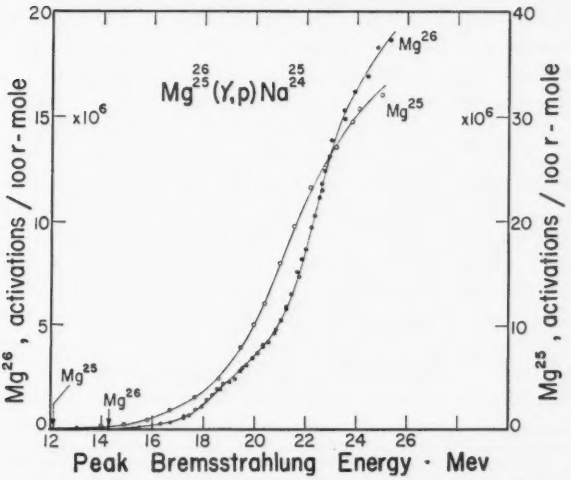

FIG. 5. Activation curves resulting from (γ, p) reactions in Mg^{25} and Mg^{26}. Note the scale on the right-hand side for the Mg^{25} curve.

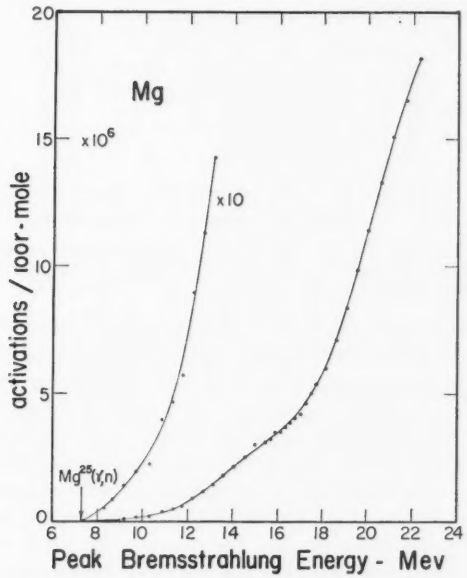

FIG. 6. Neutron yield from natural magnesium.

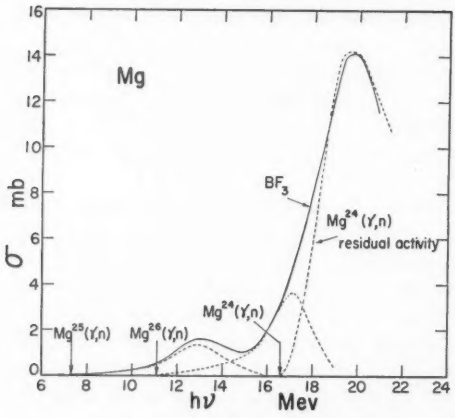

FIG. 7. Photoneutron cross section of natural magnesium (solid line). The dashed curve for Mg^{24} was obtained from the (γ, n) activation curve of Fig. 8, corrected to the isotopic abundance of Mg^{24} in the natural element. The difference between these curves represents the cross sections of the 10.1% isotope Mg^{25} and 11.1% isotope Mg^{26}.

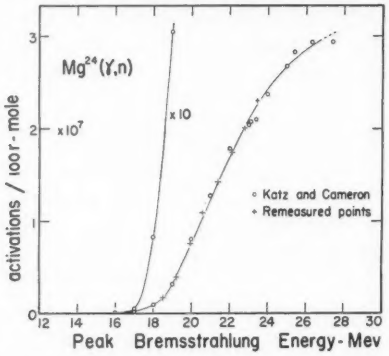

FIG. 8. Activation curve representing the (γ, n) reaction in Mg^{24} normalized according to the procedure outlined in the text. The remeasured points were taken during the course of the present experiments to check the older data of Katz and Cameron (16).

$Mg^{24}(\gamma, n)Mg^{23}$ reaction. Since it is rather difficult to normalize properly the 12 sec. activity, their result of 9.8 mbarns for the peak cross section is somewhat inconsistent with the curve of Fig. 7. In order to obtain a better value we normalized their activation curve to a value consistent with the neutron yield data at 22 Mev. from the natural element. This assumes that to a good approximation far above threshold the separate isotopes have equal neutron yields per mole per roentgen. Since Mg^{24} forms about 80% of the natural element, any deviation of the other isotope yields from Mg^{24} is reduced by a factor of 5. In our present experiment the neutron yield at 22 Mev. was found to be 1.75×10^7 neutrons/mole/100 r. This is in excellent agreement with 1.64×10^7 found by Price and Kerst (25) and 1.72×10^7 by Montalbetti, Katz, and Gol-

demberg (21). We thus normalized the (γ, n) curve to the average value of 1.70×10^7 activations/mole/100 r. This activation curve is shown in Fig. 8. As a check we repeated some of the points which are also shown in this figure. The cross section obtained from this activation curve normalized for isotopic abundance of Mg^{24} has been superposed on Fig. 7.

If the systematics of (γ, n) reactions previously found (21) apply to these reactions then one would expect the peak cross section for each of the isotopes to lie approximately 6 Mev. above threshold, except perhaps in the case of Mg^{24} which because of its very high threshold might be expected to behave more like C^{12} in which the peak cross section is only about 3 Mev. above threshold. This prediction is in fact borne out if the cross section curve of Fig. 7 is resolved as indicated by the dashed lines. The initial bump in the curve is presumed to be predominantly due to the $Mg^{25}(\gamma, n)$ cross section, while the difference between the "neutron yield" cross section and that obtained for Mg^{24} by residual activity peaks about 6 Mev. above the $Mg^{26}(\gamma, n)$ threshold and is presumed to be the cross section for this reaction.

Though the method used to resolve these cross sections has been tested experimentally and found to be quite accurate (6), to be conservative we would suggest that the peak cross sections have been established in absolute value to within a factor of 2 and the positions of the peaks to within ± 2 Mev. These two resolved cross sections corrected for isotopic abundance have been replotted in Fig. 9 where they are compared to the (γ, p) cross sections for the same isotopes.

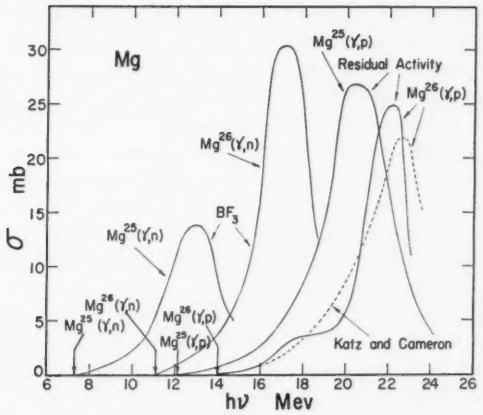

FIG. 9. Photo cross section of Mg^{25} and Mg^{26}. The (γ, p) cross section of Mg^{26} published by Katz and Cameron (16) is shown by the dashed curve.

3. DISCUSSION

(a) *Silicon*

The characteristics of the reactions in silicon as measured in these experiments, corrected for isotopic abundance, are summarized in Table III.

TABLE III

CHARACTERISTICS OF THE PHOTONUCLEAR REACTIONS IN THE SILICON ISOTOPES

Reaction	Position of peak (Mev.)	Width at half maximum (Mev.)	Maximum cross section (mbarns)	Integrated cross section to 26 Mev. (Mev-barn)
$Si^{28}(\gamma, n)Si^{27}$	20.5	3.5	21	0.075
$Si^{29}(\gamma, n)Si^{28} + Si^{30}(\gamma, n)Si^{29}$	15	3.5	23	0.096
$Si^{29}(\gamma, p)Al^{28}$	20.5	7.9	33	0.26
$Si^{30}(\gamma, p)Al^{29}$	21.5	6.1	31	0.19
$Si^{29}(\gamma, p)Al^{28} + Si^{30}(\gamma, p)Al^{29}$	21	7.2	32	0.23

Since it is not possible to resolve the (γ, n) cross sections in the Si^{29} and Si^{30} isotopes we have combined the (γ, p) cross sections in these isotopes according to their isotopic abundance. This averaged (γ, p) cross section is shown in the last line of the table and is to be compared to the average (γ, n) cross section shown in the second line.

A number of surprising facts are immediately evident from such a comparison: (*a*) the peak cross sections in the two curves are 6 Mev. apart, (*b*) the (γ, p) curves are much wider, and (*c*) the peak cross sections and integrated cross sections for the (γ, p) reaction are considerably larger than for the (γ, n) reaction. This last fact is particularly surprising since the (γ, p) threshold in these isotopes is considerably higher than the (γ, n) threshold. For better comparison, the two curves are drawn on the same diagram in Fig. 4. It is immediately evident from this diagram that the two cross sections are about equal at 17 Mev. whereas statistical theory would predict $\sigma_{\gamma,p}/\sigma_{\gamma,n} \sim 0.05$. The divergence between theory and experiment is even greater at higher energy.

In view of the above conclusions our results have been examined with great care for possible errors. The (γ, n) results are deemed to be quite reliable since they were taken relative to the $Si^{28}(\gamma, n)Si^{27}$ reaction, which was measured by Summers-Gill, Haslam, and Katz (29) using residual activity, and independently in the present experiment using the neutron detection method. The two measurements are in excellent agreement and in good agreement with the (γ, n) cross section systematics established by Montalbetti, Katz, and Goldemberg (21).

To establish the accuracy of the (γ, p) measurements it is of particular significance to point out the fact that the sum of the integrated cross section in the two isotopes for both reactions $\int(\sigma_{\gamma,n} + \sigma_{\gamma,p})\, dE$ is 0.33 Mev-barn whereas the theory of Levinger–Bethe (23) would require a minimum integrated cross section (minimum as provided by their formula) of 0.44 Mev-barn. This would indicate that our results are certainly not too large, and since the (γ, n) contribution has been quite well established, the (γ, p) integrated cross section is certainly not too large. Furthermore, the value of 0.33 Mev-barn for the sum of both reactions falls smoothly on the curve defined by the measurements of Montalbetti, Katz, and Goldemberg (21) on carbon, aluminum, cobalt, and niobium. The only values in the literature on the (γ, p) cross sections of the

silicon isotopes at the energies involved are those of Hirzel and Wäffler (11). Unfortunately their results are given relative to the (γ, n) cross section in Cu^{63}. There is wide discrepancy between their measurements on this latter isotope and those made in our laboratory, so that a comparison for the silicon isotopes would be quite meaningless.

Perlman and Friedlander (24) using 50 and 100 Mev. bremsstrahlung have measured the ratio of the proton yield from Si^{30} to the neutron yield from N^{14}. They find this ratio to be 6.6 at 50 Mev. and 5.8 at 100 Mev. At these energies the ratios of the yields of photonuclear reaction may be expected to be equal to the ratios of the integrated cross section. Johns *et al.* (14) report the integrated $N^{14}(\gamma, n)$ cross section to the peak to be 0.015 Mev-barns. If we assume that this cross section follows the usual shape and is symmetrical about the peak, the total integrated $N^{14}(\gamma, n)$ cross section is 0.03 Mev-barns. Using this value and Perlman and Friedlander's ratio we estimate the integrated $Si^{30}(\gamma, p)$ cross section to be $\sim$0.18 Mev-barns, in excellent agreement with the value of 0.19 Mev-barns reported here.

Sheline (27) has measured the ratio of the $Si^{30}(\gamma, p)$ yield relative to the (γ, n) yield in C^{12} at 35–48 Mev. and found this to be 2.7 ± 0.3. Following the procedure of the previous paragraph and using 0.05 Mev-barns for the integrated $C^{12}(\gamma, n)$ cross section (10), the integrated $Si^{30}(\gamma, p)$ cross section is estimated to be $\sim$0.13 Mev-barns. The agreement here is not quite so good but is satisfactory considering the errors involved. Sheline also measured the ratio of the proton yield in Si^{29} to that in Si^{30} at 35–48 Mev. and found it to be 1.1 ± 0.2. This agrees favorably with the ratio of the integrated cross sections for these reactions which we find to be 1.4 ± 0.2.

(*b*) *Magnesium*

The characteristics of the reactions in magnesium as measured in these experiments, corrected for isotopic abundance, are summarized in Table IV.

TABLE IV

CHARACTERISTICS OF THE PHOTONUCLEAR REACTIONS IN THE MAGNESIUM ISOTOPES

Reaction	Position of peak (Mev.)	Width at half maximum (Mev.)	Maximum cross section (mbarns)	Integrated cross section (Mev-barn)
$Mg^{24}(\gamma, n)Mg^{23}$	19.5	5.8	14.2	0.093
$Mg^{25}(\gamma, n)Mg^{24}$	$\backsim$13	$\backsim$2.7	$\backsim$14	$\backsim$0.05
$Mg^{26}(\gamma, n)Mg^{25}$	$\backsim$17	$\backsim$2.5	$\backsim$30	$\backsim$0.09
$Mg^{25}(\gamma, p)Na^{24}$	20.5	3.5	27	0.12
$Mg^{26}(\gamma, p)Na^{25}$	22	2.5	25	0.07

The values of the (γ, n) reactions in Mg^{25} and Mg^{26} are indicated as approximate according to our previous discussion and may be taken to indicate that the peak positions have been determined to within ± 2 Mev. and the cross sections to better than a factor of 2. Other values are estimated to be within our usual accuracy of $\pm 20\%$ for cross section and ± 1 Mev. for peak position.

In spite of these wide limits it is immediately evident that the peaks of the (γ, n) and (γ, p) cross sections in the same isotope are widely separated (an average of 6 Mev.) as in the case of silicon, and that there is an energy region for each isotope where the ratio $\sigma_{\gamma,p}/\sigma_{\gamma,n}$ is greater than one and is an increasing function of energy.

In view of these conclusions we will examine whether the data in Table IV are consistent with our knowledge of photonuclear reactions and previously published measurements. The element nearest in mass number to magnesium whose photonuclear properties have been measured is aluminum. Halpern and Mann (9) found the integrated (γ, p) cross section in this element to be 0.12 Mev-barn and measurements in our laboratory gave the integrated (γ, n) cross section (21) as 0.045 Mev-barn. Therefore the total integrated cross section for aluminum is 0.165 Mev-barn. This is in excellent agreement with 0.17 Mev-barn for Mg^{25} and 0.16 Mev-barn for Mg^{26} obtained from Table IV. Since integrated cross section is expected to be a smooth function of mass number, the agreement in the above values is gratifying.

The (γ, n) and (γ, p) cross sections cannot be compared separately to those of neighboring nuclei, since the ratio $\sigma_{\gamma,p}/\sigma_{\gamma,n}$ is strongly dependent on their relative thresholds and the neighboring nuclei have the (γ, p) thresholds lower than the (γ, n) thresholds. The (γ, n) cross sections have already been discussed and are presumed to have been established to better than a factor of 2. Measurements by Katz and Cameron (16) on magnesium gave the (γ, p) cross section in Mg^{26} shown by the dashed curve in Fig. 9. Except for an initial flat portion in the newer curve both cross sections are in excellent agreement to within experimental accuracy. For Mg^{25} Katz and Cameron found a peak cross section of 14.8 mbarns at 21.7 Mev. and Toms and Stephens (30) measured the same cross section using nuclear plates and found it to have a peak value of 13.7 mbarns at 20.5 Mev. with an uncertainty of the order of 50%. Our present measurements give 27 mbarns and 20.5 Mev. for these values. The positions of the peaks are in good agreement in all three measurements, but the newer cross section is considerably higher. The reason for this discrepancy is at present not known; however an examination of Fig. 9 shows that even if the $Mg^{25}(\gamma, p)$ cross section were reduced by a factor of 2 and the $Mg^{25}(\gamma, n)$ cross section were increased by a factor of 2 it would still not be possible to reconcile our results with the usual assumption of competition between neutron and proton emission from an excited nucleus.

4. QUALITATIVE ANALYSIS

Our results may be explained tentatively on the assumption that the process proposed by Courant plays a dominant role in photonuclear interactions. The following arguments will show that this assumption is not necessarily contrary to any previous experimental results and will satisfactorily account for our observations. We shall discuss the usual Goldhaber–Teller (8) and Courant (3) interactions separately.

A. Goldhaber–Teller Interaction

In this case the nucleus as a whole interacts with the incident gamma-ray

quantum forming an intermediate compound system. The excited nucleus then decays in a manner suggested by Weisskopf's statistical nucleus model.

B. Courant Interaction

The incident gamma-ray quantum interacts with a single proton in the nucleus, this proton then either (B_1) escapes giving rise to the direct photoprocess or (B_2) loses its energy by collision within the nucleus. If this latter effect occurs a compound nucleus is formed which is indistinguishable from case A. To observe the direct photoprotons it is important to suppress process (B_2) and favor (B_1); furthermore it is important that the proton/neutron ratio expected from A be small so that the observed protons may be properly identified as coming from B_1.

The proton/neutron ratio from A is small when the (γ, p) threshold is higher than the (γ, n) threshold, which is precisely the case in the isotopes investigated. Process B_2 is reduced in importance when the coulomb barrier is small favoring the escape of the direct protons. Of equal importance is that the nucleus have a large surface to volume ratio so that the proton escape is enhanced; furthermore, it is necessary that the nuclear diameter be small so that if the initial motion of the direct proton is into the interior of the nucleus, its mean free path may be commensurate with the nuclear diameter. All of these requirements are admirably satisfied by the magnesium and silicon nuclei. Previous measurements have not been conclusive since a relatively large number of protons were expected from A and in particular since process B_2 was important.

Recent measurements by Butler and Almy (2) on the (γ, n) and (γ, p) cross sections in Mo^{100} and Mo^{92} will now be examined in the light of the above discussion. For Mo^{100} they find that the (γ, p) threshold is 2.4 Mev. higher than the (γ, n) threshold; however, since this is a relatively large nucleus, process B_2 is important so that the (γ, p) cross section does not exceed the (γ, n) cross section though their ratio is about 100 times larger than expected from a statistical model calculation. For Mo^{92} the (γ, n) threshold is higher than the (γ, p) threshold by 5.1 Mev. In this case the number of protons from processes A and B_2 is expected to be quite large though again a small but definite departure from the statistical model is found.

Calculations on the shape to be expected for the direct process (γ, p) cross section indicate that it should have a resonance shape. This results from an initial portion which rises slowly because of barrier effect and a final decreasing portion falling approximately as $(h\nu)^{-7/2}$ because of the decreasing strength of interaction between the photon electromagnetic field and the proton. A very rough computation places the peak about 4 Mev. from threshold in the magnesium and silicon isotopes; experimentally the peak is found to be about 8 Mev. from the threshold. Marquez (20) has suggested that the peak should occur at about twice the threshold energy.

We must again emphasize that the above discussion is highly speculative and is only presented at this time to indicate how our experimental results may be fitted into a coherent picture.

The authors wish to thank the National Research Council of Canada for financial assistance.

REFERENCES

1. BAKER, R. G. and KATZ, L. Nucleonics, 11(No. 2): 14. 1953.
2. BUTLER, W. A. and ALMY, G. M. Phys. Rev. 89: 893. 1953.
3. COURANT, E. D. Phys. Rev. 82: 703. 1951.
4. CURTIS, N. W., HORNBOSTEL, J., LEE, D. W., and SALANT, E. O. Phys. Rev. 77: 290. 1950.
5. DIVEN, B. C. and ALMY, G. M. Phys. Rev. 80: 407. 1950.
6. GOLDEMBERG, J. and KATZ, L. Phys. Rev. 89: 1300. 1953.
7. GOLDEMBERG, J. and KATZ, L. Can. J. Phys. 32: 49. 1954.
8. GOLDHABER, M. and TELLER, E. Phys. Rev. 74: 1046. 1948.
9. HALPERN, J. and MANN, A. K. Phys. Rev. 83: 370. 1951.
10. HASLAM, R. N. H., JOHNS, H. E., and HORSLEY, R. J. Phys. Rev. 82: 270. 1951.
11. HIRZEL, O. and WÄFFLER, H. Helv. Phys. Acta, 20: 373. 1947.
12. HOFFMAN, M. M. and CAMERON, A. G. W. Phys. Rev. 92: 1184. 1953.
13. HOGG, B. G. and DUCKWORTH, H. E. Can. J. Phys. 31: 942. 1953.
14. JOHNS, H. E., HORSLEY, R. J., HASLAM, R. N. H., and QUINTON, A. Phys. Rev. 84:856. 1951.
15. KATZ, L. and CAMERON, A. G. W. Can. J. Phys. 29: 518. 1951.
16. KATZ, L. and CAMERON, A. G. W. Phys. Rev. 84: 1115. 1951.
17. LEVINGER, J. S. and BETHE, H. A. Phys. Rev. 78: 115. 1950.
18. LI, C. W. Phys. Rev. 88: 1038. 1952.
19. LI, C. W., WHALING, W., FOWLER, W. A., and LAURITSEN, C. C. Phys. Rev. 83: 512. 1951.
20. MARQUEZ, L. Phys. Rev. 81: 896. 1951.
21. MONTALBETTI, R., KATZ, L., and GOLDEMBERG, J. Phys. Rev. 91: 659. 1953.
22. MOTZ, H. T. and ALBURGER, D. E. Phys. Rev. 86: 165. 1952.
23. NUCLEAR DATA. Natl. Bur. Standards (U.S.) Circ. 499, U.S. Dept. of Commerce. 1950.
24. PERLMAN, M. L. and FRIEDLANDER, G. Phys. Rev. 74: 442. 1948.
25. PRICE, G. A. and KERST, D. W. Phys. Rev. 77: 806. 1950.
26. SEIDLITZ, L., BLEULER, E., and TENDAM, D. J. Phys. Rev. 76: 861. 1949.
27. SHELINE, R. K. Phys. Rev. 84: 1064. 1951.
28. SHER, R., HALPERN, J., and MANN, A. K. Phys. Rev. 81: 155. 1951.
29. SUMMERS-GILL, R. G., HASLAM, R. N. H., and KATZ, L. Can. J. Phys. 31: 70. 1953.
30. TOMS, M. E. and STEPHENS, W. E. Phys. Rev. 82: 709. 1951.
31. TOMS, M. E. and STEPHENS, W. E. Phys. Rev. 92: 362. 1953.
32. WEISSKOPF, V. F. and EWING, D. H. Phys. Rev. 57: 472. 1940.

THE (γ, n) AND (γ, p) CROSS SECTIONS OF ARGON^{40} [1]

By D. McPherson, E. Pederson, and L. Katz

ABSTRACT

The (γ, n) and (γ, p) cross sections in A^{40} have been measured as a function of photon energy from threshold to 24 Mev. The (γ, n) cross section was found to have a peak value of 38 mbarns at 20 Mev. and an integrated cross section of 0.35 Mev-barn. These values for the (γ, p) cross section were found to be 120 mbarns at >25 Mev. and 0.54 Mev-barn respectively. In spite of the higher (γ, p) threshold, it was found that the two cross sections were equal at 19.5 Mev. and above this energy the (γ, p) cross section became larger. This interesting result is discussed.

INTRODUCTION

Recent work in our laboratory, presented in the accompanying paper (9) (hereafter referred to as (I)), has again emphasized the importance of studying the (γ, n) and (γ, p) cross sections in the same isotope for a better understanding of the photonuclear process. Since the isotopes examined in (I) are all of low abundance in their natural element, it was felt that to emphasize the conclusion reached it would be desirable to study an isotope of high abundance.

An examination of the light weight isotopes revealed that A^{40} was the only one with the desired properties. It has an abundance of 99.6% in natural argon and its (γ, p) threshold (12.44 Mev.) is higher than the (γ, n) threshold (10.25 Mev.). Furthermore, the (γ, p) reaction results in the 55^{m} activity of Cl^{39} which may be conveniently measured by methods previously developed (6), and the (γ, n) cross section can be measured by detecting the neutrons emitted in the reaction using an apparatus described by Montalbetti, Katz, and Goldemberg (12).

EXPERIMENTAL PROCEDURE AND RESULTS

A. *The* (γ, n) *Reaction*

It is not possible to detect this reaction by residual activity measurements because of the long half life of A^{39}. However, using liquid argon samples, it was possible to detect the neutrons emitted in the reaction with the aid of the apparatus previously described (12).

The apparatus used to liquefy the argon gas is shown in Fig. 1(*a*). Liquefaction resulted when the gas was cooled with the aid of commercially available liquid nitrogen. This method is very suitable for producing liquid argon in the small quantities required. In order to prevent excessive pressure from building up in the container when it is removed from the Dewar flask, it is necessary to open the valve in the line to the atmosphere just before doing so. Closing this valve and opening the valve attached to the stainless steel container forces the liquid out. Experiments were performed with the liquid argon in a specially constructed thermos flask shown in Fig. 1(*b*).

The X-ray beam was collimated so that all of it passed through the liquid

[1] *Manuscript received May 31, 1954.*
Contribution from the Department of Physics, University of Saskatchewan, Saskatoon, Sask.

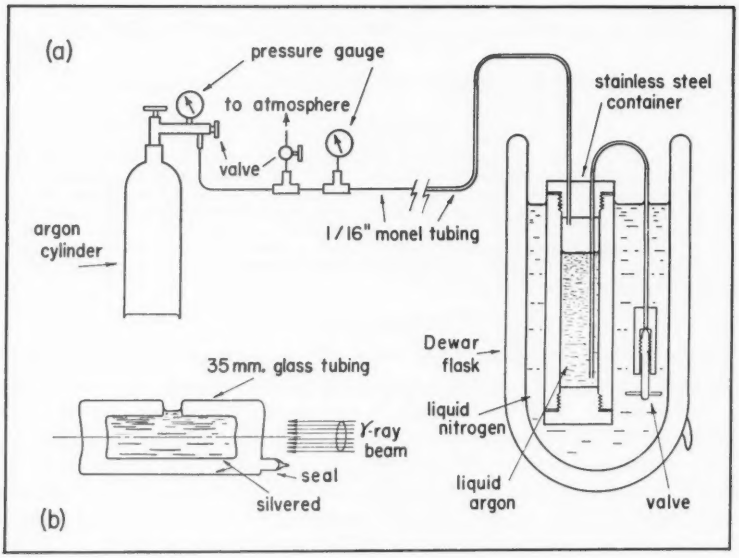

FIG. 1. (*a*) Method used for liquefying the argon gas.
(*b*) Thermos flask for holding the liquid argon during irradiation.

argon. Measurements could be carried on for about eight minutes before evaporation caused the top surface of the liquid to drop below the top edge of the X-ray beam. During this time it was possible to measure at least three points on the activation curve (Fig. 2). One precaution had to be observed in

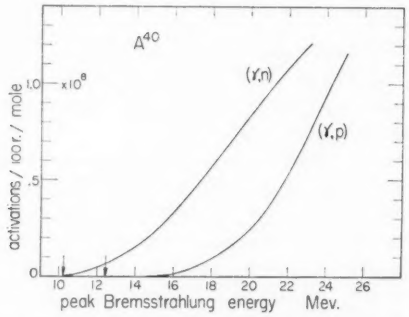

FIG. 2. Neutron yield per mole of argon per 100 r. resulting from the (γ, n) reactions, and the number of activations per mole per 100 r. resulting from the (γ, p) reactions.

these measurements; since the boiling point of argon is below that of oxygen, condensation of oxygen from the atmosphere gradually replaces the argon in the sample. To keep this effect to a minimum we replaced all the liquid in the sample container after each set of three measurements.

A dry run with the empty container in place was made to determine the neutron background. This was subtracted from the total neutron yield to give the curve shown in Fig. 2. Each point on this curve is actually the mean of four separate runs. The ordinate is given in neutron yield per mole of A^{40} per 100 roentgens of irradiation at the indicated peak bremsstrahlung energy. This normalization was made by comparison with the neutron yield from a given copper sample at 18, 20, and 22 Mev. The yield from copper had previously been well established (8) and confirmed by independent measurements in other laboratories (4, 10). The cross section was computed from Fig. 2 by the photon difference method (8) and is shown in Fig. 3.

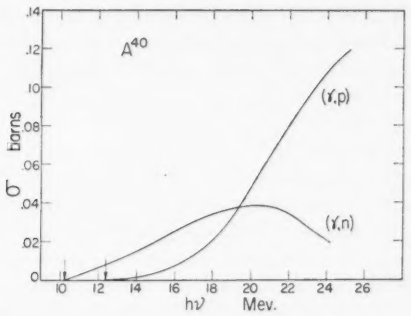

FIG. 3. Photoneutron and photoproton cross sections in A^{40} as a function of photon energy.

B. *The* (γ, p) *Reaction*

The yield from the (γ, p) reaction was measured by detecting the resulting 55^m Cl^{39} activity. Argon gas at a pressure of about two atmospheres was irradiated in an iron cylinder 8 cm. long and 8 cm. in diameter with about 1500 roentgens. The Cl^{39} formed in the (γ, p) reaction is chemically active and adheres to the cylinder walls. After irradiation the argon gas was allowed to escape and the chamber was flushed with 100 ml. of 0.006 *N* hydrochloric acid. The hydrochloric acid solution was then heated almost to boiling and 4 ml. of 0.2 *N* silver nitrate added, along with a few grains of a solid detergent to aid coagulation of the silver chloride.

The precipitate was centrifuged out, then suspended in ethanol and filtered, the resulting sample being about 15 mgm./cm.^{2} thick. The activity was measured in a standard counting arrangement. Decay curves were plotted for several samples and these samples were found to decay with a pure 55^m half life.

It was assumed that all the Cl^{39} formed in the irradiation was recovered by the above procedure. To prove that no chlorine was carried out in the gas released after irradiation, the escaping argon in one of the experiments was bubbled through dilute hydrochloric acid. No measurable activity could be detected in this solution. The exchange between chlorine atoms in the washing solution and the radioactive Cl^{39} nuclei adhering to the cylinder walls after

irradiation is, of course, very efficient because of the numerically larger number of chlorine atoms in the washing solution.

To obtain the absolute yield from the (γ, p) reaction the β activity of each sample was subject to the usual correction for self and external absorption (1) as well as for back scattering and counting geometry. The mass of each sample was calculated from the volume of the irradiating chamber and the pressure and temperature of the enclosed gas. Since the gas container subtended a fairly large angle at the X-ray target during irradiation, care was taken to properly average the angular dependence of the beam over its surface. In this manner each irradiation was normalized to the same dose rate. The yield in radioactive Cl^{39} nuclei per mole of A^{40} per 100 roentgens of irradiation is shown in Fig. 2. Each point on this curve is the average of four separate experiments. The values below 20 Mev. were reproducible to within experimental accuracy, estimated to better than 2%. Above this energy there was considerably more scattering, individual values varying by as much as 10%; the average, nevertheless, forming a smooth curve.

The cross section obtained from the activation curve is shown in Fig. 3. Starting from threshold it exhibits the slowly rising portion characteristic of charged particle reactions until the excitation energy is sufficient to overcome barrier effects, then it rises very steeply. Unfortunately, the maximum operating energy of our betatron is too low to reach the peak of this cross section. Though it would be desirable to also have the high energy end of the cross section, the portion obtained is sufficient for the present analysis.

DISCUSSION

The characteristics of the cross sections are summarized in Table I. Previous measurements (12) on various elements at 22 Mev. indicate an expected

TABLE I

CHARACTERISTICS OF PHOTONUCLEAR REACTIONS IN A^{40}

Reaction	Energy of peak σ (Mev.)	Maximum σ (barns)	$\int_0^{25} \sigma dE$ (Mev-barn)	Yield/mole/100 r. at 22 Mev.
$A^{40}(\gamma, n)$	20	0.038	0.35	1.0×10^8
$A^{40}(\gamma, n)$*	21	0.031	0.27	
$A^{40}(\gamma, p)$	>25	>0.12	0.54	0.8×10^8†

Recent measurements by Ferguson, Halpern, Nathans, and Yergin, Bull. Am. Phys. Soc. 29: No. 4, W 3. 1954.

†*Yield at 23.5 Mev.*

neutron yield of 10^8 neutrons per mole per 100 r. at $Z = 20$. By similar smooth interpolation of previous results (12) we would expect for the (γ, n) reaction a peak cross section of ~0.04 barn and an integrated cross section of ~0.3 Mev-barn. These values are in good agreement with those given in Table I. Our results are also in excellent agreement with the recent measurements by Dr. Halpern at Pennsylvania as shown in Table I. Proton yields from the (γ, p) reaction have been measured in a few elements only (5). The reported yields

in protons per mole per 100 r. at 23.5 Mev. are 0.4×10^8 for aluminum and 1.2×10^8 for nickel. Our yield of 0.8×10^8 in argon at the same energy is in excellent agreement. The sum of the two integrated cross sections is 0.89 Mev-barn. This is equal to that obtained from the equation of Levinger and Bethe (11) with $x = \frac{1}{2}$, though in this region of the periodic table the experimental values are usually about two thirds of the theoretical value.[2] For greater ease of analysis, the cross sections and their ratio are listed in Table II at 1-Mev. intervals. A plot of $\ln R$ against $(h\nu)^{\frac{1}{2}}$ yields a straight line, though the reason for this interesting behavior is not at present understood.

TABLE II

Photon energy	$\sigma_{\gamma,n}$ (mbarns)	$\sigma_{\gamma,p}$ (mbarns)	$R = \sigma_{\gamma,p}/\sigma_{\gamma,n}$
11	2.8		
12	6		
13	10		
14	14	1.5	0.11
15	20	3.4	0.17
16	26	6.8	0.26
17	30	13	0.43
18	35	21	0.60
19	37	33	0.89
20	38	49	1.26
21	37	68	1.8
22	34	84	2.5
23	26	97	3.6
24	20	107	5.3

An examination of Table II confirms the conclusions reached in (I) that it is difficult to reconcile these data with statistical theory; above 20 Mev. the (γ, p) cross section is an increasing function of energy while the (γ, n) cross section is a decreasing function. It is important to note that above 19.5 Mev. the ratio becomes greater than one so that we are not dealing with a situation investigated by a number of previous workers (2, 3, 7, 14). They were working with heavy nuclei and found that the ratio $\sigma_{\gamma,p}/\sigma_{\gamma,n}$ was greater than expected from statistical theory, though in these nuclei $\sigma_{\gamma,p} \ll \sigma_{\gamma,n}$. Thus Toms and Stephens (14) have recently measured the proton yields from foils of indium, barium, cerium, and bismuth when irradiated with 24 Mev. bremsstrahlung X-rays. They found these yields to be $\sim$1/100 of the neutron yields previously measured by Price and Kerst (13). The ratio predicted by theoretical calculations based on evaporation from a statistical nucleus was found by them to be from $\sim$1/3 to $\sim$1/100 of that observed. To explain these results Toms and Stephens analyzed the energy distribution of the observed protons and concluded that somewhat over 50% of all those emitted are the result of a direct photonuclear effect. The over-all photonuclear process is however not greatly altered by these considerations, since as mentioned above only $\sim$1% of the emitted particles are protons.

[2] *See for example Fig. 14 of Reference (12).*

In (I) we have pointed out that the evaporation model and direct photoeffect model for proton emission tend to become indistinguishable for heavy nuclei with a large volume to surface ratio and a high barrier for proton emission. Thus it is difficult to separate these two processes in the heavy nuclei used by Toms and Stephens. Argon on the other hand is a light nucleus with low barrier and large surface to volume ratio (about 70% of the nucleons are on the surface). To further emphasize the process our choice of a nucleus with $B_p > B_n$ has two effects. (i) The barrier effect combined with a high proton threshold allows the neutron cross section to turn over before the proton cross section becomes appreciable and thus brings out the difference in the (γ, n) and (γ, p) processes. (ii) Since $B_p > B_n$ we would expect even fewer protons than is usually the case, and thus the presence of a large number of protons points up the anomaly. From statistical theory we would expect that the number of emitted protons would at best equal the number of emitted neutrons at high energy. Our results however show that $\sigma_{\gamma,p}$ is greater than $\sigma_{\gamma,n}$ and is rising in value in a region where $\sigma_{\gamma,n}$ is falling with increasing energy.

The results reported in this paper and those in (I) on silicon and magnesium show that the photonuclear process, at least in these nuclides, cannot be explained on the basis of a simple evaporation theory, nor does it seem that minor modifications of existing theory will suffice.

The authors are indebted to the National Research Council of Canada for financial support and for awarding a bursary to one of them (D. Mc). They would also like to thank Dr. J. Halpern for transmitting the measurements on the (γ, n) cross section prior to publication.

REFERENCES

1. Baker, R. G. and Katz, L. Nucleonics, 11 (No. 2): 14. 1953.
2. Butler, W. A. and Almy, G. M. Phys. Rev. 89: 893. 1953.
3. Cameron, A. G. W., Harms, W., and Katz, L. Phys. Rev. 83: 1264. 1951.
4. Diven, B. C. and Almy, G. M. Phys. Rev. 80: 407. 1950.
5. Halpern, J. and Mann, A. K. Phys. Rev. 83: 370. 1951.
6. Haslam, R. N. H., Katz, L., Johns, H. E., and Moody, H. Phys. Rev. 76: 704. 1949.
7. Hirzel, O. and Wäffler, H. Helv. Phys. Acta, 20: 373. 1947.
8. Katz, L. and Cameron, A. G. W. Can. J. Phys. 29: 518. 1951.
9. Katz, L., Haslam, R. N. H., Goldemberg, J., and Taylor, J. G. V. Can. J. Phys. 32: 580. 1954.
10. Krohn, V. E., Jr. and Schrader, E. F. Phys. Rev. 87: 685. 1952.
11. Levinger, J. S. and Bethe, H. A. Phys. Rev. 78: 115. 1950.
12. Montalbetti, R., Katz, L., and Goldemberg, J. Phys. Rev. 91: 659. 1953.
13. Price, G. A. and Kerst, D. W. Phys. Rev. 77: 806. 1950.
14. Toms, M. E. and Stephens, W. E. Phys. Rev. 92: 362. 1953.

IMAGE INTERFERENCE IN CALM, NEAR-ISOTHERMAL WATER[1]

By Frederick H. Sanders

WITH AN APPENDIX

"LLOYD'S MIRROR" INTERFERENCE IN THE PRESENCE OF SLIGHT UNIFORM REFRACTION—AN APPROXIMATE THEORY

By R. W. Stewart

ABSTRACT

Some experiments are described in which strong image interference of underwater sound has been observed and measured. These effects occur frequently in coastal British Columbia waters, where calm surface conditions are common, and have been observed at frequencies close to 20 kc./sec. The observations are compared with theoretical predictions for small sound velocity gradients and reasonably good agreement obtained.

INTRODUCTION

The phenomenon of image interference is a familiar one in the fields of optics and radio. In the former, the classical "Lloyd's Mirror" experiment, wherein a beam of light striking a mirror at grazing incidence gives rise to interference fringes, is demonstrated in nearly all classrooms where elementary physics is taught. In the latter, image interference was not given much attention until the use of radiation of wavelength 10 meters and less became common. A case which has been much publicized was that of the British CH radar installations (1) which guarded the United Kingdom in the early years of World War II. The projection of radio energy over a relatively flat and highly-reflecting ocean resulted in a very complex lobal structure, and vast efforts were devoted to methods of "gap-filling" in order to eliminate the blind spots produced by the interference. In more recent years radio-astronomers (3) in Australia and other countries have made good use of the phenomenon to produce very narrow beams for the study of galactic noise.

In the case of air-borne sound, image interference is less frequently observed since large areas of high reflectivity are not commonly encountered and notes of constant pitch are rarely employed. When, however, sound is projected horizontally beneath the surface of the ocean, it is clear that interference may be expected if the frequency is constant and if the water surface appears reasonably flat to the sound radiation employed. The existence of such phenomena is discussed in *The Physics of Sound in the Sea* (4). In section 5–2–1 of this reference it is reported that image effect is usually marked at frequencies of the order of a few hundred cycles but that it is not expected to be important at frequencies above 1000 cycles. Young (6) has reported experiments in which marked interference has been observed at frequencies of a few kilocycles but, under the experimental conditions encountered, he did not observe any notable effects at higher frequencies.

[1]*Manuscript received May 20, 1954.*
Contribution from the Defence Research Board, Ottawa, Ont.

Most of the work described in References 5 and 6 was carried out in the deep ocean where, even under conditions of low or zero wind force, a good deal of swell usually exists. In the deep enclosed waters of the British Columbia coast, however, areas of flat calm water are often encountered and it is the purpose of this paper to describe remarkably consistent image interference phenomena which have been observed at frequencies near the limit of the audible range. The experiments were carried out in Nodales Channel which is highly-sheltered, over 100 fathoms deep, and through most of the year is characterized by nearly isothermal water. The oceanographic features of this area have been described in detail by Saur (5).

THEORETICAL CONSIDERATIONS

It is obvious that a pulse of sound starting from a point located between the surface and the bottom of the ocean will have a choice of several paths by which it can travel to a receiver also in the body of the water. The solid lines of Fig. 1 represent two sound rays which start from a point S in a body of iso-

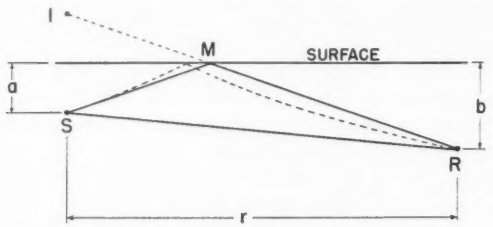

FIG. 1. Schematic representation of sound paths between two underwater points when the surface is a plane reflector. S is the source, R the receiver, and I the source image. The underwater dotted lines represents the paths under a condition of slight upward refraction.

velocity water and proceed to a point R. One ray takes the direct path SR while the other arrives via a surface reflection at M. The bottom is assumed to be too distant or too absorbent to permit reflection. By using the artifice of a virtual image at I, it is a simple matter to derive the time delay T between successive arrivals of the same sound pulse via the direct and the surface-reflected paths. If we assume that the separation r of S and R is large compared to the depths a and b we obtain for T:

$$T = 2ab/rc \qquad [1]$$

where c is the velocity of sound. Recalling that there is a phase retardation of π radians at reflection, it is clear that there will be complete interference whenever the range r satisfies the relation

$$r = 4abf/mc \qquad [2]$$

where f is the frequency and m is an integer. Interference will be constructive when m is odd, destructive when m is even. This image interference is discussed at some length in Ref. 4 and theoretical sound pressure amplitudes are derived in terms of the range, source and receiver depths, and the coefficient of surface reflection.

While the isovelocity condition is valuable as an introduction to the problem, it does not occur even in isothermal water since the velocity of sound is a function of pressure. In water whose velocity varies with depth the sound paths will be curves whose exact nature will depend on the character of the velocity gradient. The point of reflection will be displaced as indicated by the curved dotted lines of Fig. 1. The problem of formulating the law governing interference under these conditions is a good deal more difficult and has as yet not been rigorously solved even for the simple case of a pure linear gradient. Young (6) has suggested a simplification which makes an analytical expression possible in the case of curved ray paths. He bases his treatment on the argument that it is the difference in *time* of transit over the two paths that determines the relative phase of the two signals arriving at the receiver. In consequence it should be allowable to replace the curved paths by straight lines and assume that the difference in travel time along the straight paths, for a sound disturbance whose velocity is a function of depth only, is the same as it would be for a disturbance travelling over the curved paths under the same velocity restrictions. This approach yields relatively simple expressions for the time difference and, consequently, for the sound intensity distribution. The time difference T becomes:

$$[3] \qquad T = \frac{g[2a/c_0 + (b-a)/c_1] - 2ar(1/c_1 - 1/c_0)}{(a+b)}$$

where c_0 and c_1 are defined by:

$$\frac{1}{c_0} = \frac{1}{a}\int_0^a \frac{dy}{c} \quad \text{and} \quad \frac{1}{c_1} = \frac{1}{b-a}\int_a^b \frac{dy}{c}.$$

In other words, c_0 is the harmonic mean velocity between the surface and the transducer and c_1 is the harmonic mean velocity between the transducer and the receiving hydrophone. The factor "g" is given by

$$g = \sqrt{(r^2 + 4ab)} - r$$

which for r^2 large compared to the product ab reduces to $2ab/r$. Equation [3], expressed in terms of order of interference "m", becomes:

$$[4] \qquad r^2 + \frac{c^2(a+b)}{4af\Delta c}mr - \frac{cb}{\Delta c}(a+b) = 0$$

where $\Delta c = c_0 - c_1$ and $c_0 \simeq c \simeq c_1$. If $\Delta c = 0$, equation [4] naturally reduces to equation [2]. The implications of equation [4] will be discussed in relation to the experimental observations.

In an appendix to this paper (pp. 614–619) Stewart has undertaken to evaluate the time difference T between the two paths for the special but fairly common case where the sound velocity versus depth gradient is small but constant. He considers the times of transit over rays which are actually curved as in the natural situation. The only additional limitation imposed is that the angles between the ray paths and the horizontal be small. Stewart's expression for the time difference T is:

$$[5] \quad T = \frac{1}{c_s}\left[\frac{2ab}{r} + \frac{r\alpha ab}{a+b} + \frac{1}{8}\frac{\alpha^2 r^3 ab}{(a+b)^4}(4ab - (b-a)^2) - \frac{1}{16}\frac{\alpha^3 r^5 ab(b-a)^2}{(a+b)^5}\right]$$

where α is the gradient divided by the surface velocity c_s. If the harmonic mean velocities c_0 and c_1 of equation [3] are evaluated in terms of α, a, b, and c_s and the expression expanded, Young's formula for a small constant gradient becomes:

$$[6] \qquad T = \frac{1}{c_s}\left\{\frac{2ab}{r} + \frac{r\alpha ab}{a+b}\right\}.$$

It is hence apparent that only for ranges which are very large compared to the transducer and receiver depths does Stewart's expression differ materially from that of Young.

EXPERIMENTAL PROCEDURES

In September 1952 an operation was undertaken to obtain accurate measurements of the phenomenon of image interference, which was known to occur in very striking form at Nodales Channel. During the war years J. P. Tully and W. M. Cameron of the Pacific Oceanographic Group, Nanaimo, B.C., had noted and made some measurements of the effect but security restrictions prevailing at that time prevented their publication.

The present experiments were carried out from H.M.C.S. *Cedarwood* and C.N.A.V. *Ehkoli*, which are the two West Coast research vessels operated for the Defence Research Board by the Royal Canadian Navy. A taut "spacer line" between two heavy anchor clumps was first laid by *Cedarwood* so that *Ehkoli* could be secured in a fixed position without drifting or yawing. *Cedarwood* was the transmitting ship and made closing runs on *Ehkoli* from ranges of 2500 yd. to as close as was deemed safe. Sound at a frequency of 18.0 kc. was projected from a depth of approximately thirteen feet and the sound projector trained on *Ehkoli* throughout the run. Sound transmissions were emitted at a rate of five in two seconds, which at a 5-knot approach speed amounts to approximately one pulse per yard. The receiving elements were three hydrophones lowered on a single steel wire from *Ehkoli* to nominal depths of 20, 50, and 100 ft. The depth of the 100-ft. hydrophone was indicated directly by a repeating depth meter designed by J. H. Moon of Pacific Naval Laboratory. Its error, as checked in still water at Esquimalt and again at Nodales Channel, was less than one foot over the range used. The depth of the shallow hydrophone was measured by a length of light silk trout line, drawn taut. This hydrophone was visible at all times and, even when the hydrophone was streaming badly in the tidal current, it was reasonably certain that the trout line was vertical when depth measurements were made. The depth of the 50-ft. hydrophone was obtained by plotting the streaming curve of the supporting wire from the data obtained as above.

The recording equipment consisted of three logarithmic amplifiers, a four-channel oscillograph, and a Fairchild oscillograph camera. The fourth channel was used to record "radio range", i.e., a radio pulse from *Cedarwood* synchronized with the sound transmissions. The depth of *Cedarwood*'s sound projector was carefully determined both with the ship at rest and when it was steaming at 5 knots. From the above experimental arrangements, it is felt that projector

and shallow hydrophone depths were known to within 4 in. and the deeper hydrophone depths to within 1 ft. Range accuracy was ±50 ft. and the frequency was known to 100 cycles or better.

Bathythermograph casts were made from *Cedarwood*, one for each run, the location being alternated between the two ends of the course. Salinity stations were taken three times on September 10th and twice on September 11th. Eleven runs were made on the first day and ten on the second. The weather remained ideal throughout the two days, being overcast with occasional light

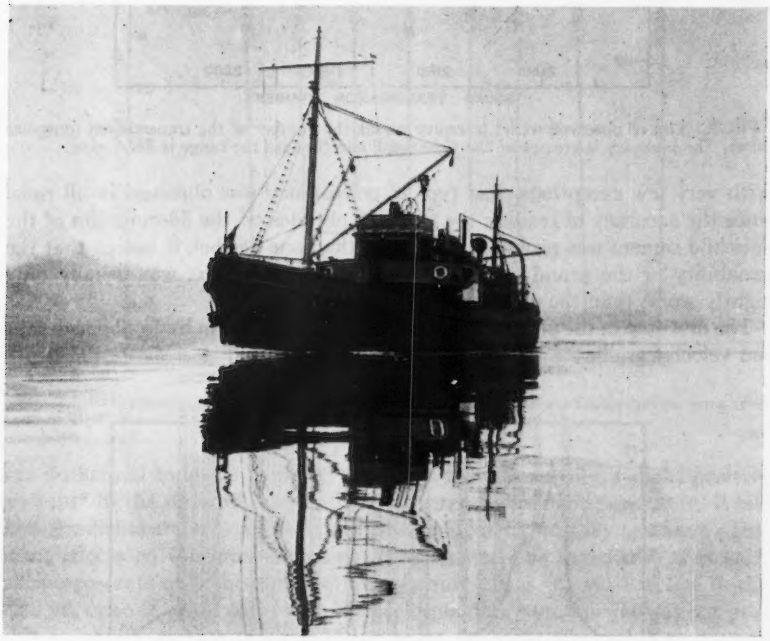

FIG. 2. Photograph taken in Nodales Channel to demonstrate the very calm surface conditions common in these enclosed waters.

showers and entirely free of wind. Fig. 2 is a photograph taken in Nodales Channel and is representative of the very calm surface conditions which so frequently prevail.

ANALYSIS OF RESULTS

The 21 runs averaged 7000 ft. in length so that, for each run, over 2000 sound pulses were received by each hydrophone. It is desired to give the reader some idea of the regular manner in which the sound intensity varies from pulse to pulse. For this purpose a 200 yd. section of Run 14 with the 100-ft. hydrophone has been plotted in Fig. 3. The range of this minimum was 1700 ft. but, for convenience, transmission number rather than range was used as the abscissa.

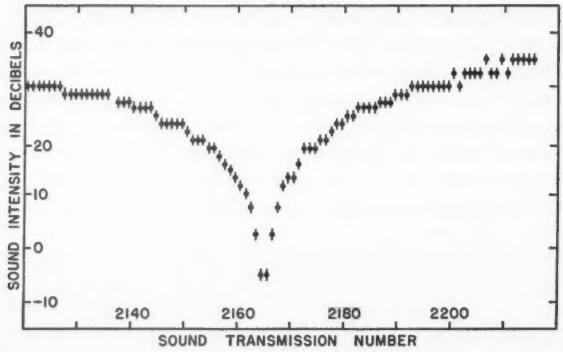

FIG. 3. Plot of observed sound intensity versus the number of the transmission (outgoing pulse). The intensity is greater at the right-hand end because the range is decreasing.

With very few exceptions, this type of consistency was observed in all runs. Since the accuracy of reading the trace amplitudes on the 35-mm. film of the Fairchild camera was probably not better than one decibel, it is seen that the variability of the sound field from one pulse to the next was usually only slightly worse than the observational error.

The first step in the analysis was to study the variation in hydrophone depths and velocity gradients over the period of the 21 runs. Fig. 4 shows the depth

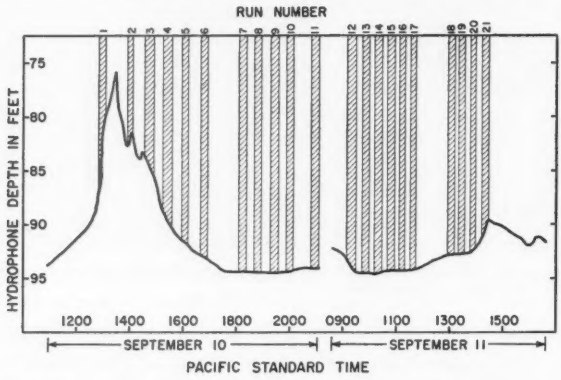

FIG. 4. Plot of the depth of the nominally 100-ft. hydrophone versus time for September 10 and 11, 1952. The shaded sections represent the times and durations of individual runs.

of the nominally 100-ft. hydrophone plotted against time over the operating period. The shaded sections represent individual runs. Around 1300 hr. on September 10th and again around 1500 hr. on September 11th, the streaming due to tidal current was quite bad. Runs 1 through 6 and 20 through 21 were discarded as being impossible to intercompare. Runs 7 through 11 on September 10th show a steady hydrophone depth but examination of the bathythermo-

graph (BT) traces for this period showed them to have a variability in structure of the order of four or five tenths of a degree between traces taken a half-hour apart. This was not expected and is attributed to "clouds" of slightly different water drifting through the channel during the "low slack" water period. The period from 0910 through 1320 on September 11th, however, showed reasonably satisfactory BT conditions from the surface to 120 ft., as demonstrated by the traces of Fig. 5. It will be noted that in all but two traces the water

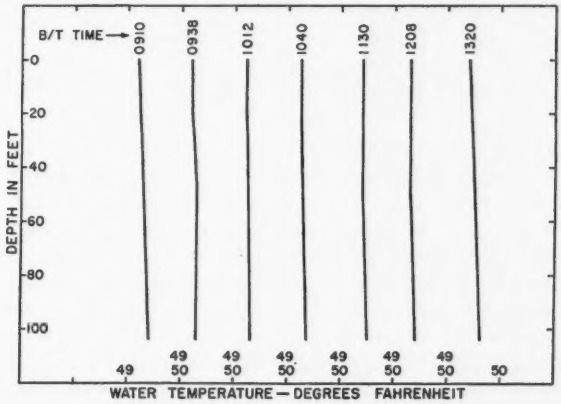

FIG. 5. Bathythermograph traces for September 11, 1952. Surface temperatures vary from 49.2° to 49.4° F.

was isothermal to 20 ft. From 20 to 100 ft. there is usually a slight positive gradient* of the order of one tenth of a degree Fahrenheit per 100 ft. While these gradients are very small, it will be shown later that they can have significant effects on the interference patterns. It must be noted also that each trace represents only the temperature structure along one vertical line in the 2000 yd. or so of water covered in the corresponding run. Since it was not possible to obtain more extensive BT coverage, it seems reasonable to assume that these seven traces represent the probable *spread* of the thermal gradients which existed over the sea paths concerned for the period 0910 to 1320 on September 11th. It is then possible to calculate the greatest and smallest velocity gradients which occurred over the four-hour period in which runs 12 through 19 were carried out.

The salinities observed at various depths over this same period were plotted against the corresponding temperatures and a salinity–temperature relation of 1.1 parts per thousand per degree Fahrenheit was established. Using Kuwahara's tables (2), the maximum and minimum values of the velocity gradient due to temperature, salinity, and pressure were computed for each hydrophone depth. From the gradients, the velocity difference Δc of equation [4] was

**In oceanography a positive temperature gradient is defined to mean that the temperature increases as the depth increases. The same convention is adopted with respect to salinity and to sound velocity.*

obtained. Table I lists the results. Since the absolute velocity enters only as a multiplying factor, the velocities c_0 and c_1 are listed as being the same and equal to 4850 ft. per sec. which was their mean value to four significant figures.

TABLE I

MAXIMUM AND MINIMUM VELOCITY DIFFERENCES

Hydrophone depth, ft.	Refractive condition	$c \simeq c_0 \simeq c_1$	$c_0 - c_1 = \Delta c$, f.p.s.
20	Max.	4850	−0.22
20	Min.	4850	−0.17
50	Max.	4850	−0.93
50	Min.	4850	−0.43
100	Max.	4850	−1.98
100	Min.	4850	−1.31

The actual sound intensities recorded by the three hydrophones for runs 12 through 19 are shown in Figs. 6, 7, and 8, where they are plotted against the logarithm of the range to avoid crowding at the short-range end. The great variation in intensity between peaks and minima is apparent in nearly all runs. Differences of 30 db. are common and in some cases they amount to 40 db. When one considers that a half-wavelength is about $2\frac{1}{4}$ in. and that the interfering signals have often traversed a half-mile of water, it appears quite remarkable that such consistent phase differences and amplitude equalities can exist. The individual extrema for the shallow and medium hydrophones are readily identifiable from run to run. While their ranges are seen to wander slightly from one run to the next, extrema of the same order can be picked

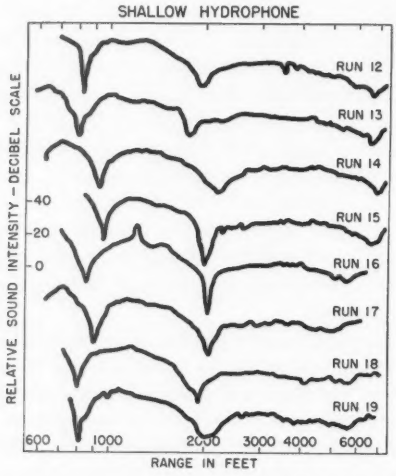

FIG. 6. Plots of sound intensity versus log range for the nominally 20-ft. hydrophone. Note the rather weak but consistent minimum between 6000 and 7000 ft. This is believed to be the "second" minimum of order $m = 2$.

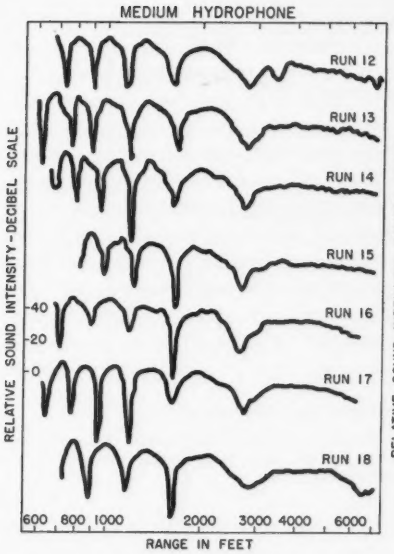

FIG. 7. Plots of sound intensity versus log range for the nominally 50 ft. hydrophone. Since the ordinate is on a decibel scale some of the minima have an intensity less than one ten-thousandth that of the adjacent maximum.

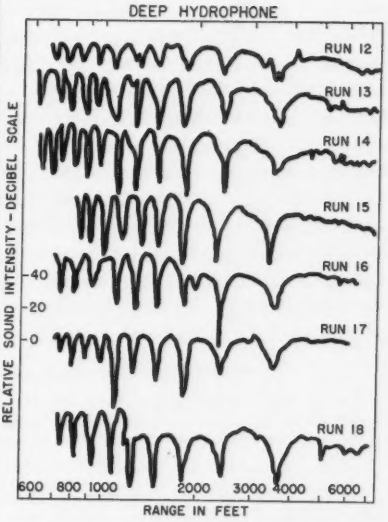

FIG. 8. Plots of sound intensity versus log range for the nominally 100-ft. hydrophone. The orders of interference range from 6 or 8 for the right-hand minimum to 28 or 30 for the extreme left-hand one. Note that no major minima exist between 4000 and 7000 ft.

out by casual inspection. Those for the deep hydrophone are more numerous and identification is a little more difficult. The question of the order of interference of the various extrema will shortly be discussed in relation to the theoretical considerations.

Before comparing the observed results with theory, it appears worth while to present a physical picture of the radiation pattern of a sound projector operating beneath a calm surface under various conditions of refraction. If the locations of the minima only, for simplicity, are displayed on a depth–range plot, from equation [2] it is clear that for zero refraction, they will lie on a series of straight lines as shown by the solid lines of Fig. 9. Each line corresponds to an even integral value of "m", i.e., to a path difference of an even number of half-wavelengths. Between these lines of complete destructive interference will lie a corresponding group of "lobes" of sound intensity whose axes would also lie on straight lines obtained by assigning *odd* values to "m" in equation [2]. If a sound receiver at a fixed range were lowered through this radiation pattern, it would indicate a series of sharp minima spaced at equal intervals in depth with strong maxima between them. Alternatively, if a receiver at a fixed depth were brought in slowly from a great range, it would indicate a series of maxima and minima starting with a maximum of order $m = 1$, which would be spaced in range according to the relation $r = km^{-1}$.

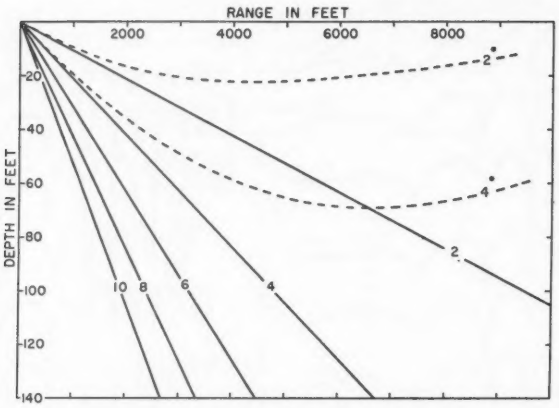

FIG. 9. Loci of the minima for a 12.9-ft. projector. The solid lines present the isovelocity condition for minima of orders 2 to 10 while the dotted curves refer to the minima of order 2 and 4 under upward refraction due to pressure alone.

If now the velocity of sound is made to change with depth, the straight-line loci of Fig. 9 will become curved. For a negative velocity gradient the curves will bend downwards and, considering destructive interference only, a receiver closing the projector from a great range will again indicate minima of orders 2, 4, 6, etc. In this case the r–m relation will be more complex than that of equation [2], but the ranges of the minima will be single-valued and must start with order $m = 2$. If, however, the gradient is a positive one, the picture becomes a great deal more interesting as indicated by the dotted lines of Fig. 9. The two curved lines marked 2* and 4* represent the loci of minima of order $m = 2$ and $m = 4$ for a velocity gradient due to pressure alone. They were obtained by inserting in equation [4] the values: $a = 12.9$ ft., $c = 4850$ f.p.s., $f = 18{,}000$ c.p.s., and values of c corresponding to a uniform gradient of 0.0182 sec.$^{-1}$.

It will be noted that a receiver 20 ft. in depth will detect *two* minima of order 2 as it approaches from a great range and that the short-range minimum occurs at a noticeably greater range than that predicted for isovelocity water, even though the velocity gradient is slight. A receiver operating at 60 ft. will detect *no* minima of order 2 but should record two of order 4. As one goes to deeper receivers the same effect will be observed, viz., disappearance of the minima of lower orders and the occurrence of two minima for each higher order. To keep the figure simple, no refracted loci have been plotted for the higher orders, but essentially the same type of upward curving occurs. The loci of Fig. 9 were obtained by the use of Young's expression. For ranges of 5000 ft. or less and receiver depths not over 100 ft., Stewart's expression (equation [5]) gives curves which lie very close to those shown. At larger ranges Stewart's curves turn up considerably more sharply, thus predicting occurrence of the second minimum at a shorter range than Young's expression. As will be seen later, however, the

interference effect at long ranges is so sensitive to slight refractive changes that successful prediction does not appear too hopeful.

A great deal of thought has been given to finding a simple way of comparing experimental observations of these complex phenomena with theoretical predictions. In Young's discussion of his observations the major emphasis has been on comparing the observed and theoretical "sound anomalies", i.e., the departure of the sound intensity from that due to simple spherical spreading. In consequence, sound intensity versus range or versus some parameter related to range has been plotted and discussed. At the high frequencies employed in the Pacific Naval Laboratory experiments, the rate of change of sound intensity with range is often very great, i.e., maxima and minima occur very close together. Any attempt to plot observed and computed intensities against range in the same figure results in a very confused picture. It was accordingly decided to deal only with ranges and orders of interference. In Fig. 10, the

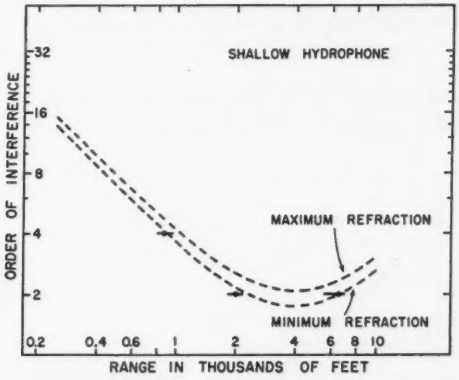

FIG. 10. Plot of log m versus log r for the nominally 20-ft. hydrophone. The solid circles are mean observed ranges for runs 12 through 19, while the bars represent the observed spread in range. The dotted curves are from Young's expression for greatest and smallest depths and refraction. With no refraction the minima should lie on the 45-degree straight lines to which the curves are asymptotic.

logarithm of order of interference has been plotted against the logarithm of the range. It is readily seen that equation [2] will yield a straight line of slope 45 degrees when integral values of "m" are plotted against "r" on the log–log scale. The intercepts of this 45-degree line will vary with the parameters of the situation. Equation [4] will yield some type of curved line with a minimum value of "m" at some definite range if Δc is negative.

The two dotted curves of Fig. 10 represent equation [4] plotted for the 20-ft. hydrophone with two sets of parameters. It will be recalled that, in the discussion of the oceanographic variables, temperature and salinity, it was concluded that the maximum and minimum refractive conditions should be considered. Inasmuch as there was an assignable uncertainty in the depths "a" and "b" of the projector and hydrophone it appeared wise to plot equation [4]

for (i) maximum values of "a" and "b" with maximum refraction and (ii) minimum values of "a" and "b" with minimum refraction. Hence the dotted curves define the limits within which the range of an extremum of given order observed by the shallow hydrophone might be expected to lie.

Looking back at Fig. 6, which gives the observed interference patterns for the shallow hydrophone, two very strong minima are observable at mean ranges of 870 and 2000 ft. These are almost certainly the "normal" minima of respective order $m = 4$ and $m = 2$. A less pronounced but quite consistent minimum is observable at about 6000 ft. This is assumed to be the second minimum of order 2. The solid circles of Fig. 10 represent the mean ranges of the three observed minima while the horizontal bars represent the spread of the observed ranges. In a broad way the agreement is good, particularly when one reflects on the small magnitude of the path difference required to produce interference and the relatively great ranges concerned. The predictions of Young's theory are quite well substantiated and, for practical purposes, it would appear that equation [4] is a useful expression for determining the general nature of the interference pattern for a shallow transmitter and receiver.

In Fig. 11 the dotted curves represent the limits within which the minima observed at the 50-ft. hydrophone might be expected to fall if equation [4] is a

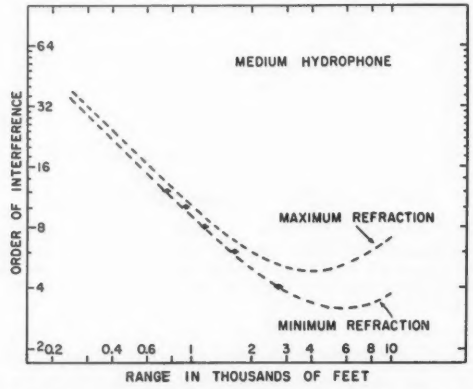

FIG. 11. Plot of log m versus log r for the nominally 50-ft. hydrophone. The reader may test other choices of order of interference by displacing the observed points up or down by two integral units. No other choice is asymptotic to a 45° line with the correct intercept.

valid expression for the ranges of the various extrema under the conditions of slight refraction observed. The solid circles represent the mean ranges of the five minima shown in the curves of Fig. 7 while the horizontal bars represent the total spread of the observed data. The assignment of order of interference is more difficult in this case than it was for the shallow hydrophone. It has been assumed that the minimum with a mean range of 2700 ft. is the "normal" minimum of order 4 and that the remainder are of orders 6, 8, 10, and 12,

respectively. The assignment of order $m = 2$ to the 2700-ft. minimum gives an unreasonably low log m–log r curve and the assignment of $m = 6$, while a little more realistic, places the whole series too high. It is unfortunate that there is no way of positively identifying the order of interference but, lacking such identification, the assumption made above seems reasonable and gives a quite good fit to equation [4]. It will be noted that, for minimum refraction, the second minimum of order 4 would be expected to occur at a range of 10,000 ft. or so. Since the ship runs usually started at a range of 6000 to 7000 ft., no data are available at this longer range. If maximum refraction had existed, no minima of order 4 would be expected.

The most spectacular and, unfortunately, the least tractable set of minima were those observed by the deep hydrophone and displayed in Fig. 8. In every run a strong and consistently broad minimum occurred at about 3600 ft. This appeared most likely to be the "normal" minimum of order $m = 8$ and the solid circles of Fig. 12 are plotted on this assumption. The open circles represent

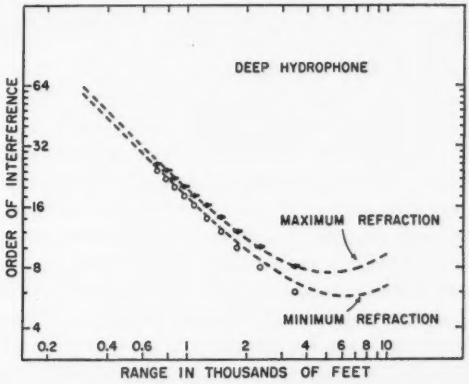

FIG. 12. Plot of log m versus log r for the nominally 100-ft. hydrophone. The solid circles represent the choice $m = 8$ for the 3500-ft. minimum while the open circles are for $m = 6$. No method is known for positively identifying the order of interference.

the same data on the assumption that $m = 6$ at 3600 ft. There is little choice between these assumptions and, consequently, no firm conclusion regarding the fit to equation [4] can be drawn.

DISCUSSION

The extent to which the ranges of the observed extrema can be compared with those predicted by theory is dependent on positive identification of the order of interference. No means for ensuring such identification are known to exist for the variable-range type of experiment just described. In the case of the data for the shallow hydrophone, however, there seems little likelihood of ambiguity. Referring once again to Fig. 10, it can be seen that any assignment of order other than that chosen would be quite unrealistic and it appears reasonable to discuss the implications of this figure.

While only three points have been plotted, these represent the mean ranges of the minima observed in eight runs. The total spread of ranges for each minimum is quite small and it is consequently felt that considerable confidence can be placed in these values. Rather less confidence can be placed in the accuracy of the temperature and salinity data which determine the velocity gradient. There is however strong evidence that the lower dotted curve represents the very minimum refractive effect possible, since it was computed for zero temperature and zero salinity gradients. It hence represents only the contribution of pressure, viz., an increase in velocity of 0.0182 ft. per sec. for each foot of depth. From the oceanographic data taken we are confident that no measurable negative temperature gradient existed over the period of runs 12 through 19. Even greater confidence is felt in the absence of any negative salinity gradient. Negative salinity gradients occur only in regions of very high evaporation rate and in British Columbia waters, with extensive fresh water being contributed by run-off throughout most of the year, positive salinity gradients are the rule. It is hence highly probable that the minimum refractive condition was greater, rather than less, than that represented by the lower dotted curve of Fig. 10.

Assuming that the above arguments are valid, it is interesting to note that the ranges of the observed minima fall consistently rather short of those predicted by theory for even the minimum refractive condition. In Fig. 11, which displays the data for the 50-ft. hydrophone, the same effect is observed. Because of the higher interference orders involved with the deeper hydrophone, there is a little more possibility of wrong assignment of order but the choice shown seems the most reasonable and again results in the observed ranges' falling very close to the curve for minimum refraction.

The first explanation for the low values of the observed ranges which occurs is that Young's theory may exaggerate the effect of refraction. Stewart's approach is however essentially rigorous for very small gradients and, at ranges up to 3000 ft., his series gives curves almost identical with those of Young. It hence appears that a fair amount of confidence may be placed in the validity of the theoretical expressions at the ranges, depths, and gradients concerned. A possible explanation of the discrepancy may be found in a natural phenomenon which has so far not been discussed, namely the motion of the water itself. If the water were moving in the direction of sound propagation at the surface but its velocity decreased or reversed with depth, the effect would be equivalent to a slight negative sound gradient. A difference of one knot between the surface and 100 ft. would just about equal the normal pressure effect. The group of runs, 12 through 19, which has been discussed was chosen to correspond to a period of low current flow, so that hydrophone streaming would be at a minimum. There is, however, a good deal of evidence to the effect that, under stronger tidal current conditions, surface water flow and deep water flow are not the same. In particular, during periods of tidal flooding, the deep water has frequently been observed to flow quite strongly towards the north while the surface water was stationary or moving slowly southwards. In general, the trend in Nodales Channel is a north-to-south flow in the surface water at most tidal periods, with deep south-to-north cur-

rents during flood periods. Runs 12 through 19 were carried out during the "high slack" and early ebb periods and, if any velocity shear existed, it would almost certainly be in the direction of an algebraic decrease in the north-south velocity with depth. Since the direction of propagation was north-to-south in all runs, this shear would result in an equivalent negative gradient. The omission of quantitative measurements of the tidal current profile was admittedly most unfortunate. It was, however, only very recently that the writer and his associates began to appreciate the probable significance of current gradient in relation to sound refraction. Lacking firm data on the tidal current velocity profile, all that can be said is that some downward refraction due to water movement is most probable and that, while this effect would be small compared to normal refraction, it would bias the ranges of the extrema in the direction observed.

CONCLUSIONS

The conclusions which may be drawn from the above experiments are the following:

(i) Under conditions of upward refraction, the image interference patterns are changed very markedly from those predicted for the isovelocity condition. For pressure refraction alone the change is so great that the simple isovelocity formula should never be used to predict the location of the extrema.

(ii) As predicted by Young and by Stewart, for conditions of upward refraction, the path difference between the direct and the reflected sound rays passes through a minimum value.

(iii) There are two results from this minimum path difference. Certain orders of interference disappear entirely and the extrema of higher order will occur at two different ranges. A limiting condition can occur where the depth of the receiver and the refraction are such that these two ranges coincide.

(iv) For relatively shallow projector and receiver depths and ranges up to 1000 yd. or so, the expressions developed by Young and Stewart are capable of giving the approximate ranges of the extrema if the velocity gradient is small. The ranges observed in these experiments tend to fall short of those predicted but it is felt that this discrepancy is very probably attributable to a variation in tidal current with depth.

(v) For shallow projectors and receivers and ranges greater than 1000 yd., the locations of the extrema are so sensitive to small changes in refraction that prediction of their location is not too hopeful.

ACKNOWLEDGMENTS

It must be appreciated that experiments of the type described are possible only through the co-operation and earnest individual efforts of many people. The writer wishes to acknowledge his indebtedness to the scientists, technicians, and computers of Pacific Naval Laboratory, to the commanding officers and ships' companies of H.M.C.S. *Cedarwood* and C.N.A.V. *Ehkoli*, and to the oceanographers and technicians of Pacific Oceanographic Group. Special thanks are due Dr. R. W. Stewart, Dr. W. N. English, and Mr. H. L. Grant of Pacific Naval Laboratory for many stimulating discussions.

REFERENCES

1. CROWTHER, J. G. and WHIDDINGTON, R. Science at war. Philosophical Library Inc., N.Y. 1948. p. 19.
2. KUWAHARA, S. Hydrographic review, 16 (2): 123. 1939.
3. LAVELL, B. and CLEGG, J. A. Radio astronomy. Chapman and Hall, Ltd., London. 1952. p. 184.
4. Physics of sound in the sea. Summary Technical Report of Division 6, National Defence Research Committee, 8: 95. 1946.
5. SAUR, J. T. F., JR. U.S. Navy Electronics Laboratory Report No. 188. Problem 2A5, June 12, 1950. Unclassified.
6. YOUNG, R. W. J. Acoust. Soc. Amer. 19(1): 1. 1947.

Appendix

"LLOYD'S MIRROR" INTERFERENCE IN THE PRESENCE OF SLIGHT UNIFORM REFRACTION—AN APPROXIMATE THEORY

1. *Introduction*

Young's theory (6) of mirror interference in the presence of refraction takes account of the variation in the velocity of propagation but assumes an incorrect path in that it neglects the curvature of the rays. While intuitively the approximation appears reasonable if the curvature is small, the limits of its applicability are not immediately obvious.

The curvature of the path has three effects:

1. The actual path length is greater than the straight line path.
2. The average velocity of propagation is greater than along the straight line path.
3. The point of reflection is displaced if the source depth differs from the receiver depth.

An exact solution in the general case of a stratified medium appears very difficult. However, if the simplifying assumption of a constant velocity gradient is made, an approximate solution may be obtained in a reasonably straightforward manner. A comparison of the results of this solution with those of Young's theory under the same conditions of a uniform velocity gradient should serve as a guide to the reliability of Young's theory under the more general conditions of a variable velocity gradient.

2. *Definitions*

We shall use a Cartesian co-ordinate system:

x increases as the range increases from $x = 0$ at the source S.

y increases as the depth increases from $y = 0$ at the surface (see Fig. 13).

$y = a$ at the source S.

$y = b$ at the receiver R.

$x = r$ at R.

$x = x_1$ at the point of reflection.

$x_2 = r - x_1$.

C = velocity of sound, a function of y only.

C_0 = velocity at the surface.

C_1 and C_2 are respectively the sound velocities at S and R.

$C = C_0(1 + \alpha y)$ where α is constant if the velocity gradient is uniform.

θ = angle of sound ray with horizontal.

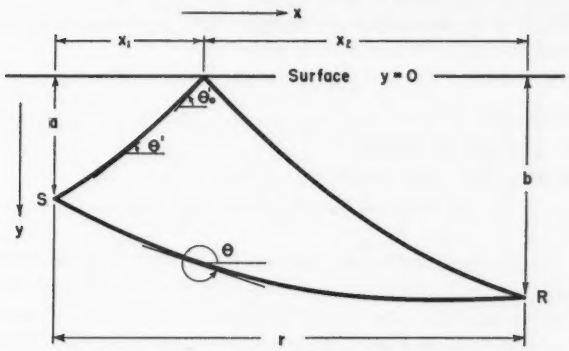

FIG. 13. This is essentially the same schematic drawing as Fig. 1 but indicates the nature of the quantities used to develop Stewart's expression.

$\theta = \theta_0$ at the point of reflection.

t = time of progression of a wave front along the ray.

The surface reflected path is designated by primed quantities.

From Snell's Law:

$$\frac{d\theta}{d\xi} = \frac{\cos\theta_0}{C_0}\frac{dC}{dy} = \alpha\cos\theta_0$$

where ξ is an element of length along the ray.

3. *Assumptions*

1. All angles are small so that

$$\cos\theta = 1 - \tfrac{1}{2}\theta^2, \qquad \sin\theta = \theta - \tfrac{1}{6}\theta^3, \qquad \tan\theta = \theta + \tfrac{1}{3}\theta^3, \text{ etc.}$$

(Note that this implies that x is large compared with a and b and the approximation breaks down at very short ranges.)

2. α is of such a magnitude that αx is of the order of, or smaller than, the maximum value of $|\theta|$. Therefore αa and αb are of the order of or less than the maximum value of θ^2.

3. $d\theta/dx = \alpha$ may be used in place of $d\theta/d\xi = \alpha\cos\theta_0$. (This amounts to assuming that the *change* in $\cos\theta$ along any ray is negligible in terms involving $d\theta/dx$.)

4. That the point of reflection $x = x_1$ may be obtained as follows:

A direct solution for x_1, while theoretically possible since a, b, r, and α fully determine the position, involves solution of a rather complicated cubic equation, yielding a result not readily approximated. We shall thus make use of the following device.

To a first approximation it is in general true that if η is a function of γ

(i) $$\eta = \eta_0 + [f(\eta) - f(\eta_0)]/f'(\eta_0)$$

where $\eta = \eta_0$ and $df/d\eta = f'(\eta_0)$ when $\gamma = 0$ provided $f(\eta)$ and $f'(\eta)$ are continuous functions of η near $\gamma = 0$.

If α is small it is reasonable to suppose that x_1 has a value not greatly different from the value where $\alpha = 0$, which is

$$ar/(a + b).$$

We thus choose $\gamma = \alpha$, $\eta = x_1$, $f(\eta) = (a/x_1) - (b/x_2)$ in equation (i) and use the first approximation only.

To a first approximation (assuming $\sin\theta = \theta$)

$$a/x_1 = \theta_0' - \tfrac{1}{2}\alpha x_1, \qquad b/x_2 = \theta_0' - \tfrac{1}{2}\alpha x_2,$$

therefore
$$\frac{a}{x_1} - \frac{b}{x_2} = \frac{-\alpha}{2}(x_1 - x_2) = f(\eta) \doteq \frac{-\alpha r}{2(a+b)}(a - b),$$

and
$$f(\eta_0) = 0.$$

Also
$$\frac{d}{dx_1}\left(\frac{a}{x_1} - \frac{b}{x_2}\right) = -\frac{a}{x_1^2} + \frac{b}{x_2^2} = f'(\eta),$$

therefore
$$f'(\eta_0) = \frac{-(a+b)^2}{r^2}\left(\frac{1}{a} + \frac{1}{b}\right) = \frac{-(a+b)^3}{abr^2}.$$

Thus

$$x_1 = \frac{ar}{a+b} + \frac{\alpha}{2}\frac{abr^3}{(a+b)^4}(a - b)$$

$$= \frac{ar}{a+b}\left\{1 + \frac{\alpha}{2}\frac{br^3}{(a+b)^3}(a - b)\right\}. \tag{ii}$$

4. To find the time t required for a wave front to travel from S to R by the direct path, we use

$$t = \int_0^r \frac{1}{C\cos\theta}\,dx,$$

but by Snell's Law $\dfrac{C}{\cos\theta} = \text{const.} = \dfrac{C_1}{\cos\theta_1}$ on any path. Therefore

$$t = \frac{\cos\theta_1}{C_1}\int_0^r \frac{1}{\cos^2\theta}\,dx \tag{iii}$$

where θ_1 and C_1 are the angle and speed respectively of the wave front at S.

By assumption 3

$$\theta = \theta_1 + \alpha x.$$

Substituting in equation (iii) and using assumption 1 gives

$$t = \frac{\cos\theta_1}{\alpha C_1}\int_c^r \frac{1}{\cos^2(\theta_1 + \alpha x)}\,d(\theta_1 + \alpha x)$$

$$= \frac{\cos\theta_1}{\alpha C_1}\tan(\theta_1 + \alpha r) - \tan\theta_1,$$

$$t = \frac{1}{\alpha C_1}(\alpha r + \tfrac{1}{2}\theta_1^2\alpha r + \theta_1\alpha^2 r^2 + \tfrac{1}{3}\alpha^3 r^3). \tag{iv}$$

To maintain the order of approximation, it is sufficient to put

$$\theta_1 = \frac{b-a}{r} - \frac{\alpha r}{2}.$$

Hence

$$t = \frac{r}{C_1}\left[1 + \frac{(b-a)^2}{2r^2} - \frac{\alpha(b-a)}{2} - \frac{\alpha^2 r^2}{24}\right]$$

$$= \frac{r}{C_0}\left[1 + \frac{(b-a)^2}{2r^2} - \frac{\alpha(b+a)}{2} - \frac{\alpha^2 r^2}{24}\right]. \quad \text{(v)}$$

In equation (v), the first term on the right side represents the time to cover the horizontal distance; the second is the ordinary Lloyd Mirror approximate term to account for the slant of the path; the third term shows the effect of the variation in velocity assuming a linear path; and the last term is the effect of the curvature of the ray.

5. For the surface reflected path:

Using equation (v) for each section of the path,

$$t' = \frac{1}{C_0}\left[x_1 + \frac{a^2}{2x_1} - \frac{\alpha a x_1}{2} - \frac{\alpha^2 x_1^3}{24} + x_2 + \frac{b^2}{2x_2} - \frac{\alpha b x_2}{2} - \frac{\alpha^2 r^3}{24}\right].$$

Substituting for x_1 and x_2 as in equation (ii) gives

$$t' = \frac{1}{C_0}\left[r + \frac{(a+b)^2}{2r} - \frac{\alpha r(a^2+b^2)}{2(a+b)} - \frac{\alpha^2 r^3 ab(a-b)^2}{4(a+b)^4} - \frac{1}{24}\frac{\alpha^2 r^3(a^3+b^3)}{(a+b)^3} - \frac{1}{16}\frac{\alpha^3 r^5 ab(a-b)^2}{(a+b)^5}\right]. \quad \text{(vi)}$$

6. Thus

$$\Delta t = t' - t \quad \text{(vii)}$$

$$= \frac{1}{C_0}\left[\frac{2ab}{r} + \frac{\alpha r ab}{a+b} + \frac{1}{8}\frac{\alpha^2 r^3 ab}{(a+b)^4}\{4ab-(a-b)^2\} - \frac{1}{16}\frac{\alpha^3 r^5 ab(a-b)^2}{(a+b)^5}\right].$$

Each term on the right-hand side of equation (vii) is of the same order if we assume that αr is of the order of a/r (assumption 2).

The first two terms of this expression are the same as those given by Young (6) if his result is reduced to the order of approximation used here. The terms in $(a-b)^2$ describe the effect of the shift in the point of reflection, and the remaining term gives the effect of the curvature of the path.

7. There are four relevant parameters in equation (vii), viz., a, b, r, and α. However, these are not completely independent in their effects, and by multiplying through by αC_0, and substituting $\alpha a = A$, $\alpha b = B$, $\alpha r = R$, we get:

$$\alpha C_0 \Delta t = \frac{2AB}{R} + \frac{RAB}{A+B} + \frac{1}{8}\frac{RAB}{(A+B)^4}[4AB-(A-B)^2] - \frac{1}{16}\frac{R^5 AB(A-B)^2}{(A+B)^5}. \quad \text{(viii)}$$

We may thus plot, for example, curves of constant $\alpha C_0 \Delta t$ (which are curves of constant difference in phase) on a graph of B vs. R with A as a parameter. Three such graphs are shown in Figs. 14, 15, and 16. The particular values of

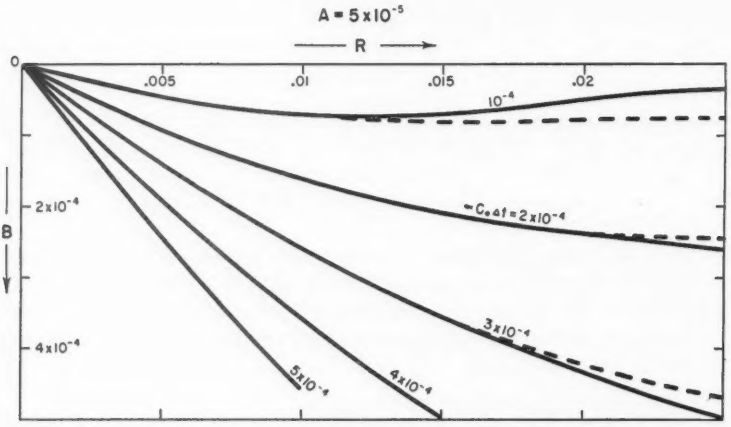

FIG. 14. This plot is analagous to Fig. 9 but uses the dimensionless parameters R, A, and B. For pressure refraction alone and a sound velocity of 4850 f.p.s., $A = 5 \times 10^{-5}$ represents a projector depth of approximately 13 ft. The range corresponding to $R = .02$ would be near 5300 ft.

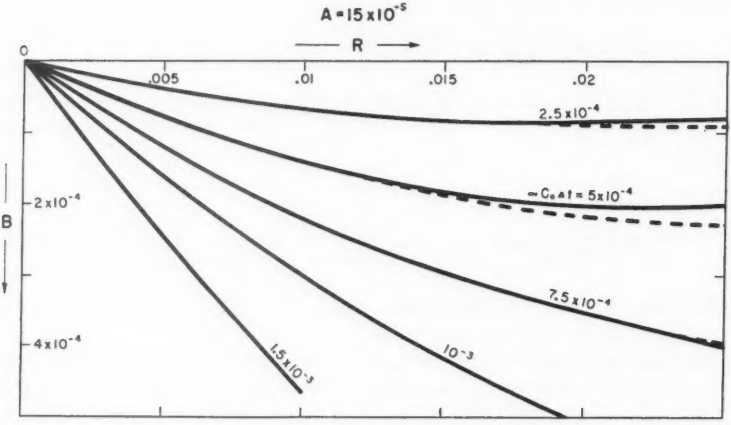

FIG. 15. Plot of R versus B for $A = 15 \times 10^{-5}$. For pressure refraction alone and a sound velocity of 4850 f.p.s., this would represent a projector depth of approximately 40 ft.

A chosen are such that the graphs are representative of the effect when a is of the order of 10 to 100 ft. and α is of the same order as that produced by pressure alone in sea water. The full lines are the results of the whole expression of equation (viii).

Except at large values of R the first two terms of the expression dominate. The effect of considering only these two terms is shown dotted where it differs appreciably from the complete expression. The difference between these two lines is an indication of the accuracy of Young's approximation.

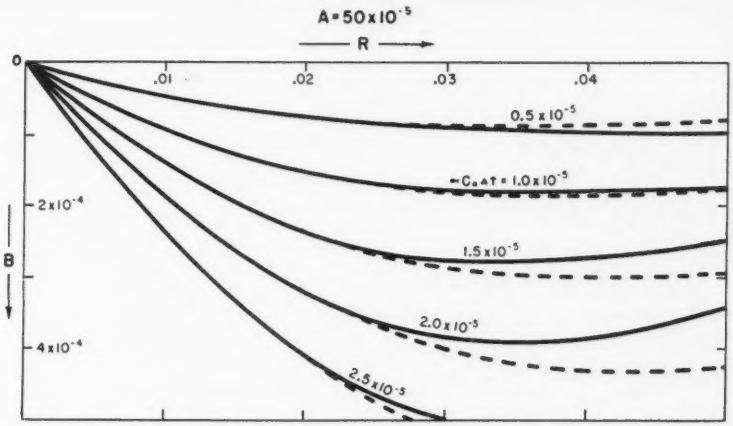

FIG. 16. Plot of R versus B for $A = 50 \times 10^{-5}$. For pressure refraction alone and a sound velocity of 4850 f.p.s., this would represent a projector depth of approximately 130 ft.

CANADIAN JOURNAL OF PHYSICS

Notes to Contributors

Manuscripts

(i) ***General.*** Manuscripts should be typewritten, double spaced, on paper 8½×11 in. **The original and one copy are to be submitted.** Tables (each typed on a separate sheet) and captions for the figures should be placed at the end of the manuscript. Every sheet of the manuscript should be numbered.

Style, arrangement, spelling, and abbreviations should conform to the usage of this journal. Names of all simple compounds, rather than their formulas, should be used in the text. Greek letters or unusual signs should be written plainly or explained by marginal notes. Superscripts and subscripts must be legible and carefully placed.

Manuscripts should be carefully checked before they are submitted; authors will be charged for changes made in the proof that are considered excessive.

(ii) ***Abstract.*** An abstract of not more than about 200 words, indicating the scope of the work and the principal findings, is required, except in Notes.

(iii) ***References.*** References should be listed **alphabetically by authors' names,** numbered, and typed after the text. The form of the citations should be that used in this journal; in references to papers in periodicals, titles should not be given and only initial page numbers are required. All citations should be checked with the original articles and each one referred to in the text by the key number.

(iv) ***Tables.*** Tables should be numbered in roman numerals and each table referred to in the text. Titles should always be given but should be brief; column headings should be brief and descriptive matter in the tables confined to a minimum. Numerous small tables should be avoided.

Illustrations

(i) ***General.*** All figures (including each figure of the plates) should be numbered consecutively from 1 up, in arabic numerals, and each figure referred to in the text. The author's name, title of the paper, and figure number should be written in the lower left corner of the sheets on which the illustrations appear. Captions should not be written on the illustrations (see Manuscript (i)).

(ii) ***Line Drawings.*** Drawings should be carefully made with India ink on white drawing paper, blue tracing linen, or co-ordinate paper ruled in blue only; any co-ordinate lines that are to appear in the reproduction should be ruled in black ink. Paper ruled in green, yellow, or red should not be used unless it is desired to have all the co-ordinate lines show. All lines should be of sufficient thickness to reproduce well. Decimal points, periods, and stippled dots should be solid black circles large enough to be reduced if necessary. Letters and numerals should be neatly made, preferably with a stencil (**do NOT use typewriting**), and be of such size that the smallest lettering will be not less than 1 mm. high when reproduced in a cut 3 in. wide.

Many drawings are made too large; originals should not be more than 2 or 3 times the size of the desired reproduction. In large drawings or groups of drawings the ratio of height to width should conform to that of a journal page but the height should be adjusted to make allowance for the caption.

The original drawings and one set of clear copies (e.g. small photographs) are to be submitted.

(iii) ***Photographs.*** Prints should be made on glossy paper, with strong contrasts. They should be trimmed so that essential features only are shown and mounted carefully, with rubber cement, on white cardboard.

As many photographs as possible should be mounted together (with a **very** small space between each photo) to reduce the number of cuts required. Full use of the space available should be made and the ratio of height to width should correspond to that of a journal page; however, allowance must be made for the captions. Photographs or groups of photographs should not be more than 2 or 3 times the size of the desired reproduction.

Photographs are to be submitted in duplicate; if they are to be reproduced in groups one set should be mounted, the duplicate set unmounted.

Reprints

A total of 50 reprints of each paper, without covers, are supplied free. Additional reprints, with or without covers, may be purchased.

Charges for reprints are based on the number of printed pages, which may be calculated approximately by multiplying by 0.6 the number of manuscript pages (double-spaced typewritten sheets, 8½ × 11 in.) and making allowance for illustrations (not inserts). The cost per page is given on the reprint requisition which accompanies the galley.

Any reprints required in addition to those requested on the author's reprint requisition form must be ordered officially as soon as the paper has been accepted for publication.

Contents

Page

Gamma Radiation from the Proton Bombardment of Oxygen—*J. B. Warren, K. A. Laurie, D. B. James, and K. L. Erdman* - - 563

Reflection from a Wire Grid Parallel to a Conducting Plane—*James R. Wait* - 571

The Photoneutron and Photoproton Cross Sections of Silicon and Magnesium—*L. Katz, R. N. H. Haslam, J. Goldemberg, and J. G. V. Taylor* - 580

The (γ, n) and (γ, p) Cross Sections of Argon^{40}—*D. McPherson, E. Pederson, and L. Katz* - - - - - - - - - - - - - - - 593

Image Interference in Calm, Near-isothermal Water—*Frederick H. Sanders. With an Appendix* "Lloyd's Mirror" Interference in the Presence of Slight Uniform Refraction—An Approximate Theory—*R. W. Stewart* - - - - - - - - - - - - - - - - 599

Printed in Canada *by* University of Toronto Press